Theoretical and experimental perspectives in utilizing nanobubbles as inhibitors of corrosion and scale in geothermal power plant

Kioka, Arata
Department of Earth Resources Engineering, Kyushu University

Nakagawa, Masami
Department of Mining Engineering, Colorado School of Mines

出版情報：Renewable and Sustainable Energy Reviews. 149 (111373), 2021-10. Elsevier
バージョン：
権利関係：

Published from Renewable and Sustainable Energy Reviews (2021)
https://doi.org/10.1016/j.rser.2021.111373

Theoretical and experimental perspectives in utilizing nanobubbles as inhibitors of corrosion and scale in geothermal power plant

Arata Kioka*
Department of Earth Resources Engineering, Kyushu University, Fukuoka 819-0395, Japan.
*Correspondence to: kioka@mine.kyushu-u.ac.jp (A. Kioka)
Masami Nakagawa
Department of Mining Engineering, Colorado School of Mines, Golden, CO 80401, USA.

ABSTRACT:

Corrosion and scaling have presented serious technical challenges to make geothermal power reliable and affordable. Due to the large quantities of geothermal water that must be processed to obtain heat, many conventional chemical inhibitors are not economically viable. Moreover, most chemical inhibitors are costly and can readily change the fluid chemistry that results in generating undesired products. Nanobubbles are environment-friendly, inexpensive, and easy-to-use, and thus have been used in a broad area of applications by taking advantage of their unique physicochemical properties. Here we propose that nanobubbles can be used as inhibitors of corrosion and scaling in the geothermal system. First, this paper reviews the mitigation methods for corrosion and scale currently used in a geothermal power system, and second, provides an overview on the novel use of nanobubbles as inhibitors of corrosion and scale from theoretical and experimental perspectives. We suggest that nanobubbles can be powerful, chemically benign, environment-friendly, and inexpensive inhibitors of corrosion and scaling, compared with the chemical products commonly used. The mechanisms on how nanobubbles act as inhibitors and their inhibition effectiveness vary with different chemical conditions of geothermal fluid.

HIGHLIGHTS

- Conventional mitigation methods for corrosion and scale in the geothermal system are reviewed.
- The novel usage of nanobubbles as a “green” inhibitor for corrosion and scale is discussed.
- Nanobubbles can be an effective, environment-friendly, and inexpensive inhibitor of corrosion and scaling.

KEYWORDS

Nanobubbles; Corrosion inhibitor; Scale inhibitor; Calcium carbonate scale; Silica scale; Geothermal energy

Received 31 December 2020; Received in revised form 18 May 2021; Accepted 14 June 2021
https://doi.org/10.1016/j.rser.2021.111373

1. Introduction

The energy landscape is changing, especially in Japan where nuclear power plants facing challenges to be reopened. As a necessary measure, coal-fired power plants are filling the gap in energy needs; however, support for it is facing international challenges. A significant opportunity for justifying the development of geothermal power plants is emerging. This is because geothermal power plants produce much less greenhouse gas emissions and present much fewer operational risks compared to conventional fossil fuel and nuclear power plants [1]. In geothermal power plants, however, degradation of the pipes due to corrosion and scale formation are major economic concerns in addition to the high initial costs. The degradation of pipes eventually leads to efficiency loss and eventual failure of the system. In the geothermal industry, the acceptable corrosion rate is set below 0.1 mm/year to maintain the health of the 20-year life of a power generation system. However, intensive corrosion is possible in steel pipes when the acidic geothermal fluid at moderate-to-high temperatures is used [2]. Dissolved CO_2, H_2S, NH_3, and chloride ions in the geothermal fluids lead to corroding metallic materials. The corrosion rate in an acidic geothermal fluid ranges from a couple of millimeters per year in the moderate fluid environment to several hundred millimeters per year in the high-temperature and high-fluid velocity environment [3]. When acidic geothermal water is to be used, it is inevitable to expect increased operational costs of geothermal facilities. Corrosion can also significantly intensify by temperature decrease or oxygen ingress along with time-dependent procedures on operation and maintenance for equipment in geothermal power plants [4]. Interruption of continuous geothermal power production to replace and repair the damaged piping systems can result in huge economic losses, and often do so unexpectedly.

The formation of scale in the geothermal power plant system is another critical and unavoidable problem. The estimated cost due to problems associated with scale formation in the geothermal industry worldwide is about $27 billion a year [5–7]. Scale is formed by various operating factors such as temperature, pressure, pH, flow velocity, degree of supersaturation, and presence of other salts and ions interfering in solution [8]. The most common scale formations in the geothermal power plant are calcium carbonate and silica. Scale formation of calcium carbonate is dominant in the low and moderate temperature fluids. Silica scaling is common in high-enthalpy geothermal power plants, where fluids are rapidly cooled during geothermal energy production [1,9]. The rates of silica scaling in silica-rich geothermal power plants reported worldwide mostly range between 600 and 4,500 $mg/m^2/day$ (e.g. [10–12]). A numerical calculation of power output in the geothermal power plant shows that factoring in such scaling significantly reduces the resulting output [13]. The scale formation increases fluid resistance resulting in extra energy consumption. Moreover, intense scale formation can cause irreparable damage due to clogging in the pipes of plant equipment as well as in the injection wells.

Numerous efforts have been made to mitigate corrosion and scale formation in the geothermal power plant. These mitigation methods are usually either the correct selection of pipe materials and/or chemical additives. Inhibiting scale formation is still challenging due

to the very complex nature of the scale formation process, and adapted methods are mostly either too costly and/or environmentally unacceptable. This review paper presents a state-of-the-art method of the usage of nanobubbles as environment-friendly and inexpensive inhibitors instead of chemical additives. Fundamental research of nanobubbles, stable spherical gas packages having a typical diameter of 50–200 nm within a liquid, is still in its infancy [14], yet successful applications are growing in broad disciplines [15]. Numerous studies have revealed that nanobubbles have not only unique physicochemical properties [16] but also very broad applications including water treatment [17,18], cleaning [19], high-density hydrogen storage [20], and promoting the metabolism of living organisms [21,22]. In particular, nanobubbles represent a promising ability to mitigate fouling on surfaces [19] that can be utilized in the geothermal system. Recently, nanobubbles are sought as inhibitors of corrosion and scale formation for solving geothermal problems. For example, immersion tests with continuous injection of nanobubbles in acidic geothermal water on-site a geothermal power plant reveal their effectiveness for inhibiting mild-steel corrosion [23]. The study also suggests that their inhibition effectiveness for silica scale formation may vary with the pH of geothermal water. Therefore, the effectiveness of nanobubbles as the inhibitors of corrosion and scale formation of calcium carbonate and silica in various chemical conditions should be investigated based on theoretical views and experimental studies. In this paper, we first review conventional mitigation methods for corrosion and scale formation, and second, review the novel usage of nanobubbles as an effective “green” inhibitor for corrosion and scaling on the surface inside the pipes and equipment in the geothermal system.

2. Conventional methods for mitigation

2.1. Corrosion mitigation

Well-planed material selection and corrosion inhibiting engineering are prerequisites to reduce the severity of corrosion. In geothermal systems, for example, most corrosion is observed in carbon steel pipes and equipment under any conditions of geothermal fluid. The use of mild-carbon steel invites severe damage in highly corrosive geothermal fluids. In contrast, titanium, nickel and high nickel-based alloys, and (super-)ferritic and (super-)austenitic stainless steels are expensive but used in some equipment because they yield higher resistance to most geothermal fluid environments [3]. Nevertheless, selecting the right materials is very challenging because of the high cost of highly resistant materials and the varying nature of geothermal fluids, even in a single operating day. Although the mitigation solutions deep inside the wellbore are complicated in terms of extreme pressure and temperature conditions, other corrosive environments are on the surface where several mitigation solutions are generally available. Thus, in addition to the corrosion-resistant materials, numerous studies have sought after chemical solutions or coating a thin layer of certain materials on the metal surface for inhibiting corrosion. Metallic corrosion in an aqueous solution consists of the anodic dissolution of metals and cathodic reduction of oxidants in the solution. In an acidic system, the main corrosion process comprises:

$Fe \rightarrow Fe^{2+} + 2e^{-}$ (Anodic oxidation) and

$2H^{+} + 2e^{-} \rightarrow H_2$ (Cathodic reduction)

Corrosion inhibitors can generally be classified as anodic inhibitors, cathodic inhibitors, and mixed inhibitors [24,25]. A protective coating of the material surface has also been found to be effective for inhibiting corrosion, by using micro-arc oxidation (MAO) technologies [26] and organic compounds such as oxadiazoles [27], several Schiff base compounds [28], triazines, acetylenic alcohols, propargyl alcohol, and their derivatives [29,30], Pyridazinium derivatives [31], Imidazole and Imidazoline derivatives [32] (Table 1; see Finšgar & Jackson [29] for more details and references therein). These organic coatings represent significant inhibition of corrosion, most achieving the effectiveness of corrosion inhibition of 80–98% even in the acidic solution. However, the use of these organic materials in the geothermal fluid has some intrinsic shortcomings such as easy degradation, susceptibility to solvents and high temperature, and weak adhesion to metal substrates. Alternatively, several researchers have developed inorganic and composite coatings to prevent metals from corroding. For example, diamond-like carbon film prepared by the plasma-enhanced chemical vapor deposition method and sol-gel silica coatings on the stainless-steel surface with thicknesses of 50–300 nm function physical barriers and restrain from the surface [33,34]. Nanostructured silica films using the liquid-phase deposition method on the metal stainless steel substrate present good anti-corrosion measures, while some shortcomings are also recognized in thin silica films [35]. A coating of the 150-μm thick poly(phenylene sulfide)- (PPS-)montmorillonite (MMT) clay nanocomposite adequately protects the carbon steel in a simulated geothermal fluid at 300°C. Ning et al. [36] studied anticorrosion

efficiency of low-energy inorganic silica coatings on copper substrates with thicknesses of 200–300 nm prepared by the liquid phase deposition method in geothermal water at 90°C. The corrosion inhibition efficiency reached around 40%, while the anticorrosion could be reduced when the silica coating is immersed for a period longer than 24 hours because the coating was subject to peeling from the metal surface [36]. There have also been numerous works undertaken for studying plant extracts as effective "natural" corrosion inhibitors due to the toxic nature of synthetic organic and inorganic inhibitors and their high cost [37,38]. It should be noted, however, most of the reported organic, inorganic, and plant-based inhibitors were examined either at low temperatures, in the short testing periods, or in the static conditions without the presence of fluid flow (e.g., Table 1). On the other hand, scaling accompanies corrosion of mild steels at moderate temperatures in geothermal power plants and helps the resistance of the steels [39]. Several studies have further found that the initial layer formation of amorphous silica precipitates prevents the underlying steel surface from further reaction with geothermal fluid [36,40,41]. Therefore, silica precipitates may indeed act as a corrosion inhibitor in an acidic moderate-temperature geothermal fluid, while controlling the magnitude of precipitation is difficult.

The pH is known for being one of the most significant factors determining the severity of corrosion in the geothermal fluid [42,43]. For example, Yanagisawa et al. [43] reported the corrosion rate of carbon steel in the geothermal fluid is 1.6 mm/yr at pH 3.6 and 145°C while the rate is reduced to around 0.1 mm/yr at higher pH of 4.6 and higher temperature of 168°C. Thus, the pH adjustment using chemical materials is conventionally one of the common methods for inhibiting such intensive corrosion. Yet, it can easily change the fluid chemistry that can produce undesired products, and their corrosion inhibition effectiveness is generally not satisfactory. Therefore, there is a demand of the pH adjustment for corrosion inhibition without the use of chemical materials.

Table 1: Examples of the methods for corrosion mitigation in the previous studies.

Methods	Inhibition effectiveness	Conditions (e.g., solutions, temperatures, materials)	Testing period
MAO coatings [26]	91 – 97%	0.1 M NaOH or 1 M HCl; 15 – 25°C; Al alloy	~1 h (Lab)
Oxadiazoles [27]	87 – 98%	1 M HCl; 30°C; mild steel	24 h (Lab)
	49 – 69%	0.5 M H_2SO_4; 30°C; mild steel	24 h (Lab)
Schiff base compounds [28]	Up to 93%	20 mM HCl; Room temperature; mild steel (SS400); constant stirring	5 d (Lab)
Propargyl alcohol [29]	19 – 72%	15% HCl; 28±2°C; N-80 steel	0.5 – 6 h (Lab)
	77 – 98%	15% HCl; 28±2°C; cold rolled mild steel	0.5 h (Lab)
	97 – 99%	15% HCl; 30°C & 105±5°C; mild steel	6 h (Lab)
Pyridazinium derivative [31]	27 – 95%	1 M HCl; 25°C; Mild steel	6 h (Lab)
Imidazoline derivative [32]	95 – 97%	15% HCl; 25°C; Low carbon steel (St37-2)	6 h (Lab)
Sol-gel silica coatings [33]	99%	1 N H_2SO_4; 80°C & 200°C; AISI 304 stainless steel	N/A (Lab)

Diamond-like carbon films [34]	99%	3.5% NaCl; AISI 304 stainless steel	20 – 60 min (Lab)
Nano-silica coatings [36]	Up to 40%	Geothermal water; 60°C; Red copper	24 h (Lab)

2.2. Scale mitigation

2.2.1. Calcium carbonate scale

Calcium carbonate ($CaCO_3$) scale formation occurs according to the following reactions:

CO_2 (g) ↔ CO_2 (aq),

CO_2 (aq) + H_2O (l) ↔ H_2CO_3 (aq),

H_2CO_3 (aq) ↔ H^+ (aq) + HCO_3^- (aq),

HCO_3^- (aq) ↔ H^+ (aq) + CO_3^{2-} (aq),

$Ca^{2+} + CO_3^{2-} \leftrightarrow CaCO_3$ (s) ↓

Calcium carbonate scale formation generally occurs in the production well as a result of changes in pH and pressure associated with boiling processes as fluid rises to the surface. An increase in pH of fluid encourages the conversion of bicarbonates (HCO_3^-) to carbonates (CO_3^{2-}), resulting in forming calcium carbonate. Andritsos and Karabelas [44] showed an increase of pH from 8.8 to 10 produced 6 times greater deposition of calcium carbonate. Although the effect of temperature is not significant, the precipitation increases with higher surface temperature and increases exponentially at temperatures over 60°C [6]. Given the temperature of geothermal fluid, calcite is the most stable crystal calcium carbonate structure and the most common mineral in the calcium carbonate scale.

Scale inhibitors are usually dispersants that keep scales from adhering tightly to piping or equipment surfaces. Great strides have been made for mitigation of calcite scale formation, by ion exchange softening, acid dosing, chemical inhibitors, pH modifications, metal ions, electromagnetic radiations, ultrasound, and surface modifications, and they show the scale inhibition effectiveness of generally 30–90% [6,45,46]. The migration methods of calcite scale effect either by reducing the amount of calcium carbonate formation or inhibiting the growth of calcium carbonate crystals. The conventional methods of mitigation by adding chemical inhibitors include organophosphates [47], humic acid [48], amino trimethylene phosphonic acid (ATMP), polyamine polyether methylene phosphonate (PAPEMP) [49], ethylenediaminetetraacetic acid (EDTA) [50], and metal ions [51]. The polyelectrolytes such as poly(acrylic acid) (PAA) [6,49], poly(maleic acid) (PMA) [52] and poly(methacrylic acid) (PMAA) and poly(acrylic acid-co-2-acrylamide-2-methyl-propane sulfonic acid) (PAA-PAMPS) [53] are also used for inhibiting calcium carbonate scale. These inhibitors adsorb to growing calcium carbonate crystals and bind to the growth sites. This results in inhibiting the crystal growth and destruct the regular shape of the calcite crystal, leading to the weakening of crystal stability [49]. These methods are among the most commonly used [54], representing good inhibition effectiveness of 50–90% (Table 2).

212 However, these inhibitors should be used with very low dosages for mitigating hard scale
213 deposits. Also, calcium calcite scaling can be accompanied by simultaneous corrosion [55]. If
214 used with high dosages, these inhibitors become uneconomical, and they can either
215 promote undesirable corrosion or coagulate calcium carbonate promoting deposition of
216 even soft deposits that make a rapid reduction of fluid flow [56]. Therefore, studying
217 optimum amounts of these inhibitors is essential for effective migration of calcium
218 carbonate scaling.

219 It has also been shown that the process of scale formation depends on surface
220 properties as well as bulk solution and operating conditions. Low-energy surfaces will
221 reduce the adhesion force between calcium carbonate and metal surface significantly
222 [57,58]. Thus, several works have studied inorganic nanoparticles and nanomodified
223 surfaces for inhibiting calcium carbonate scale by lowering surface free energies [36,51,58].
224 Nano-coatings by TiO_2 and SiO_2 with nanometer-thick layers prepared by low surface free
225 energies on the substrates showed effective inhibition of calcium carbonate scaling [36,59]
226 (Table 2), highlighting potential applications in mitigating calcium carbonate scaling.
227
228 **Table 2:** Examples of the methods for calcium carbonate scale mitigation in the previous
229 studies.

Methods	Inhibition effectiveness	Conditions (e.g., solutions, temperatures, materials)	Testing period
Ultrasound [46]	62 – 76%	pH = 8.5; 25°C	N/A (Lab)
Organophosphates [47]	~20 – 30%	pH = 8.3 – 8.9; 20°C	18 hours (Lab)
Humic acid [48]	Up to 99%	pH = 8.5; 25°C	100 min (Lab)
PAA	7 – 21% [6]	pH = 10.0; 25°C	3 hours (Lab)
	< 73% [6]	pH = 7 – 8; 70 – 120°C	5 hours (Lab)
	< 56% [49]	6.4 mM Ca^{2+} & 12 mM HCO_3^-; 60°C; bubbling	5 hours (Lab)
ATMP [49]	< 49%	6.4 mM Ca^{2+} & 12 mM HCO_3^-; 60°C; bubbling	5 hours (Lab)
PAPEMP [49]	< 60%	6.4 mM Ca^{2+} & 12 mM HCO_3^-; 60°C; bubbling	5 hours (Lab)
EDTA [50]	N/A (inhibited)	pH = 8.0 – 9.0; 60 – 230°C; Constant stirring	48 hours (Lab)
PMA [52]	< ~90%	Sea water; pH = 10.4 – 10.7; room temperature	40 min (Lab)
PAA-PAMPS Copolymers [53]	> 90%	pH = 7; 25°C	75 min (Lab)
Iron(III) [6]	Up to 99%	pH = 7.0 – 8.0; 15 – 35°C	20 min (Lab)
Magnesium [6]	N/A (inhibited)	pH = 8.0 – 9.0; 25°C	N/A (Lab)
Nano-metal-phosphonates [51]	20 – 35%	pH = 10.0 – 10.8; 25°C	7 hours (Lab)
Nano-silica coatings [36]	40 – 60%	Geothermal water; 40°C	7 days (Lab)
	20 – 40%	Geothermal water; 60°C	7 days (Lab)
	55 – 60%	Geothermal water; 90°C	7 days (Lab)

Nano-TiO_2 coatings [59]	N/A (inhibited)	20°C	67 hours (Lab)

2.2.2. Silica scale

Silica concentration in 200–350°C aquifer waters in the geothermal system generally falls within 300–700 mg/kg SiO_2, and it is dominantly controlled by quartz solubility [60,61]. In the geothermal environment, this silica scaling problem is of the same importance as metallic corrosion. In most geothermal systems, geothermal fluid at a temperature greater than 180°C is equilibrium with quartz, and soluble silica is present mostly in non-ionic form as monosilicic acid $Si(OH)_4$ at low concentrations and acidic to neutral pH. Silica dissolution involves a chemical reaction shown as [62]:

$$SiO_2 + 2H_2O \leftrightarrow Si(OH)_4$$

Silica scaling occurs via two major processes: chemisorption and polymerization. Chemisorption, direct deposition of silica monomers on surfaces, occurs very slowly while polymerization, silica monomers coagulating to nano-scale polymer particles, often occurs rapidly [63]. The monosilicic form undergoes polymerization when concentration increases, through dehydration to form the polysilicic acids that are connected by silica-oxygen bonds. In the mildly acidic to basic conditions, polymerization is proceeded according to the reaction given by [64–66]:

$$Si(OH)_4 + OH^- \leftrightarrow (OH)_3SiO^- + H_2O,$$

$$Si(OH)_3^- + Si(OH)_4 \rightarrow (OH)_3Si - O - Si(OH)_3 + OH^-,$$

$$2n\ (OH)_3Si - O - Si(OH)_3 \rightarrow \text{Cyclic/Colloidal Silica} \rightarrow \text{Polymeric silica (scale)}.$$

In the presence of metal ions, certain metal silicate complexes form in geothermal brines. Silica scale formation is significantly enhanced by the presence of alumina, aluminum iron, iron hydroxides, and ferrous and ferric irons [67–71]. Thus, amorphous silicates may precipitate rapidly through condensation polymerization reactions of aluminum-silica and iron-silica complexes according to their stoichiometry [72]:

$$2M(OH)_3 + xSi(OH)_4 \rightarrow M_2O_3 \cdot xSiO_2 + (2x + 3)H_2O$$

where M is Al and Fe. Silica minerals exhibit prograde solubility and their saturation reaches with respect to amorphous silica during cooling between 100°C and 200°C, resulting in fast precipitation and subsequent rapid deposition.

Silica scale in geothermal power plants occurs as often as calcium carbonate scale does. However, mitigation techniques of silica scale are generally less effective than those of calcium carbonate scale. Nevertheless, numerous studies during the last two decades have found certain effectiveness in brine acidification methods and chemical additives for mitigating silica scale. The brine acidification method is found to be effective in mitigating hisingerite (iron(III) phyllosilicate) scaling by adding sulfuric acid. Minimizing the brine acidification is necessary because acidification adjustment can exacerbate metal corrosion [73,74]. In contrast to calcium carbonate scale inhibition, most of the chemical additives including 1-Hydroxyethane 1,1-diphosphonic acid (HEDP), 2-Phosphonobutane 1,2 4-

tricarboxylic acid (PBTC), boric acid, polyelectrolytes such as poly(acrylic acid) (PAA) and poly(maleic acid) (PMA) show poor scale inhibition effectiveness generally less than 10% [66]. Furthermore, the use of PAA, while it is found to be effective for mitigating calcium carbonate scale, needs careful consideration into its amount because PAA forms the Al-PAA complex in the presence of aluminum, resulting in adsorb on the silica surface and rather accelerating the formation of silica scale [75]. Other chemical additives such as quicklime, aril-type dimethyl-aril ammonium chloride (DAMAC) [76], Polyethyleneimine (PEI), polyallylamine hydrochloride (PAH) [77], dimethyl diallyl ammonium chloride (DADMAC), poly(acrylamide-*co*-diallyl dimethylammonium chloride) (poly(AM-*co*-DADMAC)) [77], cationic inulin (CATIN) polymer [78], polyvinyl pyrrolidone (PVP) [79] and microporous polypropylene membrane distillation [80] generally show good scale inhibition effectiveness (Table 3).

Another technique of silica scale mitigation is the application of coating. Most coating methods are expensive but are effective in preventing silica scaling. A variety of paints including oil-based paints, water-based paints, and their combination coatings have been found to show protective performance, while water-based coatings have less performance than two combinations containing an epoxy resin topcoat [81,82]. Sugama et al. [82–84] studied Poly(phenylene sulfide) (PPS) containing polytetrafluoroethylene (PTFE) as an antioxidant additive, silicon carbide as a thermally conductive filler, and aluminum oxide-rich calcium aluminate (ACA) as an abrasive wear-resistant filler (Table 3). The PTFE-blended PPS coatings play a role in anti-scaling barriers on the carbon steel tubes in the harsh geothermal environment containing silica-rich brine. Although the coating methods represent a perfect scaling inhibition effectiveness, the effectiveness of protective coating depends on the pretreatment of the surface and the properties of fluid.

Table 3: Examples of the methods for silica scale mitigation in the previous studies.

Methods	Inhibition effectiveness	Conditions (e.g., solutions, temperatures, materials)	Testing period
Brine pH modification [74]	Up to 99%	Geothermal water; pH = 7.0; SiO_2 = 850 g/m^3	28 days (On site)
HEDP [66]	4 – 9%	pH = 7.0; 230°C; Constant stirring	22 hours (Lab)
PBTC [66]	6 – 8%	pH = 7.0; 230°C; Constant stirring	22 hours (Lab)
Boric acid [66]	8 – 10%	pH = 7.0; 230°C; Constant stirring	22 hours (Lab)
PAA [66]	2 – 4%	pH = 7.0; 230°C; Constant stirring	22 hours (Lab)
PMA [66]	1 – 2%	pH = 7.0; 230°C; Constant stirring	22 hours (Lab)
Quicklime [76]	17 – 98%	Geothermal water; pH = 8.7 – 10.9; 90°C	2 hours (On site)
DAMAC [76]	22 – 64%	Geothermal water; pH = 8.7 – 10.9; 90°C	2 hours (On site)
PEI [77]	30 – 55%	pH = 7.0±0.1; constant stirring	72 hours (Lab)
PAH [77]	35 – 65%	pH = 7.0±0.1; constant stirring	72 hours (Lab)
DADMAC [79]	52 – 86%	Geothermal water; pH = 6.5 – 6.6; 90°C; constant stirring	15 min (On site)

	24 – 83%	Geothermal water; pH = 8.3; 90°C; constant stirring	15 min (On site)
Poly(AM-co-DADMAC) [77]	31 – 61%	pH = 7.0±0.1; constant stirring	72 hours (Lab)
CATIN polymer [78]	51 – 67%	pH = 7; constant stirring	8 hours (Lab)
PVP [79]	9 – 22%	Geothermal water; pH = 8.3; 90°C; constant stirring	15 min (On site)
Membrane distillation [80]	N/A (inhibited)	pH = 4 – 11; 60°C	50 hours (Lab)
PTFE-blended PPS coatings [82,83]	Up to 100%	Geothermal water; 89 – 109°C	45 days (On site)

3. Properties of nanobubbles as an inhibitor of corrosion and scaling

Since the first hypothesizing the existence of nanobubbles in 1994, they have been researched in a broad range of disciplines, with an emphasis on understanding their behavior in aqueous solutions [14]. Nanobubbles can be observed in the form of either free-floating (i.e., bulk nanobubbles), surface pinning (surface nanobubbles), or nano-pancakes. Unlike micrometer-sized bubbles (microbubbles), the remarkable properties of nanobubbles are their longevity in aqueous solutions and stability at high temperatures. Nanobubbles have less buoyancy due to their size, and their rise velocity is very slow because their movement is governed by random Brownian motions [85,86]. The electrostatic interactions between nanobubbles are significant and discourage their coalescence [86]. Nanobubbles can survive for many hours, several days, or even a couple of months [87–89] rather than microseconds expected theoretically [90]. Furthermore, the stability of nanobubbles is insensitive to the pH of the aqueous solution [91]. Surface nanobubbles have also been recognized to make a strong impact on the solid-liquid interface as they change the two-phase contact to a three-phase contact. This includes the effect of surface nanobubbles that can change the wettability and slippage on the solid surface [92–96]. Also, surface nanobubbles are stable with respect to an increase in temperature up to the boiling point of water because they can pin a micro-droplet from the receding water over the surface [97]. Furthermore, surface nanobubbles also yield superstability — they are stable under a large reduction of water pressure down to −6 MPa [98]. Thus, the use of nanobubbles enables optimizing the surface condition through hydrodynamic controlling of the solid interface, allowing a broad range of geothermal applications. Furthermore, the use of nanobubbles will benefit in preventing chemical pollution and reducing cost for maintaining geothermal infrastructure, compared with the chemical products commonly used in geothermal industries.

In the past decade, bulk nanobubbles have been generated by numerous methods such as cavitation, electrolysis, ultrasonication, and temperature gradients [99–104]. The cavitation method is used most often for nanobubble generation [105] through several mechanisms including hydrodynamic [106], acoustic [107], particle [108], and optical cavitations [109]. A dispersion of hydrodynamic cavitation nanobubbles can be collected in light of the difference in the rising velocity. Microbubbles disperse rapidly up to gas-liquid surface due to their buoyancy and burst, while nanobubbles remain in solution because of their Brownian behavior. Thus, it takes time to obtain nanobubbles and lacks control of bubble size and uniformity [110]. Instead, ceramic membranes with uniform nanometer pores can generate uniform and size-controllable nanobubbles [110,111]. The typical diameter of generated nanobubble is proportional to the pore size of the ceramic membrane [110]. Their number densities generally range from 10^6 to 10^{11} bubbles per milliliter (mL), with a typical number density of 10^8 bubbles per mL [14]. The species of gases (e.g., air, nitrogen, oxygen) can be freely chosen by injecting into the ceramic device. A recent ceramic-type nanobubble generator can control not only the bubble size by changing

the injection pressure [110] but also the number density of bubbles by changing the rotational speed of the carbon-ceramic column (Figure 1).

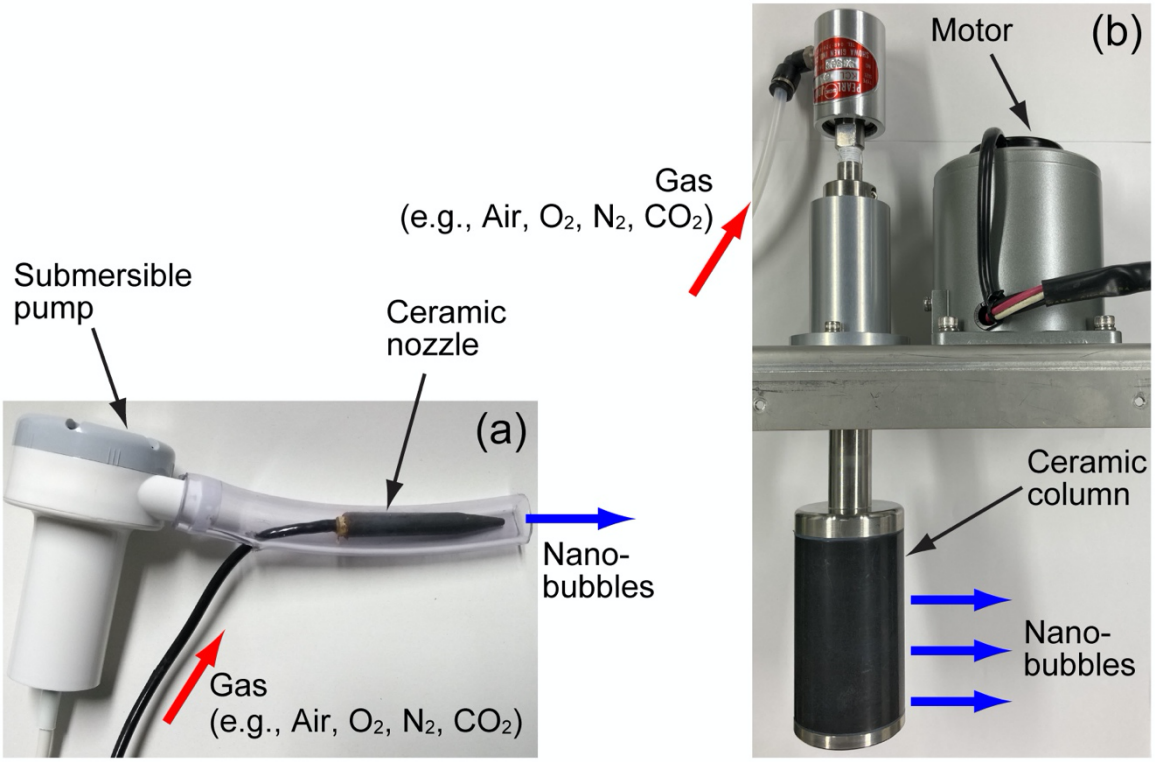

Fig. 1. Nanobubble generators (Anzaikantetsu, Co. Ltd., Yokohama, Japan). (a) Ultrafine pore ceramic-nozzle type nanobubble generator [23]. This device can generate on the order of 10^9 bubbles per milliliter with a mean diameter of 85 nm. (b) Ultrafine pore ceramic column-rotational type nanobubble generator which can generate a higher concentration than the nozzle type generator (Figure 1a).

Fine gas bubbles can exert a significant influence on the fluid flow along the hydrophobic, micro-structured surfaces by changing the friction of liquid flow on the surface. The hydrodynamic boundary condition at solid walls is generally represented by a slip length of a flowing liquid at a solid interface. The slip length of liquid at the interface, λ, is expressed by $u = \lambda(\partial u/\partial z)_{z=0}$, where u is the slip velocity at the solid wall and $(\partial u/\partial z)_{z=0}$ is the velocity gradient at the wall in the normal direction [112], indicative of a larger slip length with a lower drag of liquid flow at the interface. It is known from several experiments that a slip length of water over hydrophobic surfaces normally does not exceed 100 nm [113–117]. Nevertheless, previous theoretical and experimental works have found that the presence of surface nanobubbles has a profound impact on the slip length on a hydrophobic surface, although the slippage is also influenced by roughness and wettability on the surface [92,93,95]. Molecular dynamics modeling also suggests the slip length can be 10 µm with the presence of nanobubbles on the hydrophobic surfaces [93,118]. As the height of the nanobubbles increases, the slip length increases on a surface that is

intermittently or completely covered with nanobubbles [94]. Moreover, nanobubbles favor being pinned and staying for a long time on a rough surface [94,96], encouraging to increase the slip length. Consequently, the surface nanobubbles act as a “bubble mattress” which reduces friction and chemical reaction against the flowing fluid on the surface [119]. These properties benefit in that nanobubbles are much more stable on the hydrophobic rough surface than larger bubbles are, and that the surface nanobubbles can influence the fluid flow along the steel surface for a relatively long time. Thus, the use of nanobubbles could be more valuable than general superhydrophobic coatings if the effectiveness of anti-corrosion and anti-scaling by using nanobubbles is similar to that by using the superhydrophobic coatings. The coating materials are more subject to peeling from the surface [36,59].

Another possible important role of nanobubbles is serving as a dispersant or helping flotation of scale particles. The gas-water interfaces are generally negatively charged [120]. The stability of bulk nanobubbles reviewed above may be attributed to the presence of a surface charge exerting an external electrostatic pressure to balance the internal Laplace pressure [121]. The Derjaguin-Landau-Verwey-Overbeek (DLVO) theory describes the interaction of colloidal particles and aggregation behavior [122]. Zeta potential, an important parameter in the DLVO theory, represents the electrostatic potential of the surface of the particle. The zeta potential describes ion adsorption and double layer interactions between charged particles, representing the potential stability of the colloid system. In general, all particles in suspension repel each other and avoid aggregation of particles in a colloidal dispersion when they have a large positive or negative zeta potential. The nanobubbles will thus be stabilized by strong repulsion forces avoiding their coalescence at a high absolute value of zeta-potential. An approximate boundary between stable and unstable dispersions of nanobubbles can be at an absolute value of zeta potential of 30 mV [123]. The zeta potential of nanobubbles shows a sigmoidal profile with pH. Nanobubbles are positively charged in the acidic solutions, while they generally have a negative surface charge at normal pH values (Figure 2) [19,100,101,121,124–127] because of the preferential adsorption of hydroxide OH^- ions in the first molecular layers of water at the gas-liquid interface [128,129]. This suggests that the surface nanobubbles may play a role as dispersant when the nanobubbles and scale particles (i.e., calcium carbonate and silica) are charged similarly. In contrast, the bulk nanobubbles charged oppositely to scale particles may be attached to scale particles [101,130–132], probably helping flotation of scale particles to prevent the deposition and formation of scale on the steel surface.

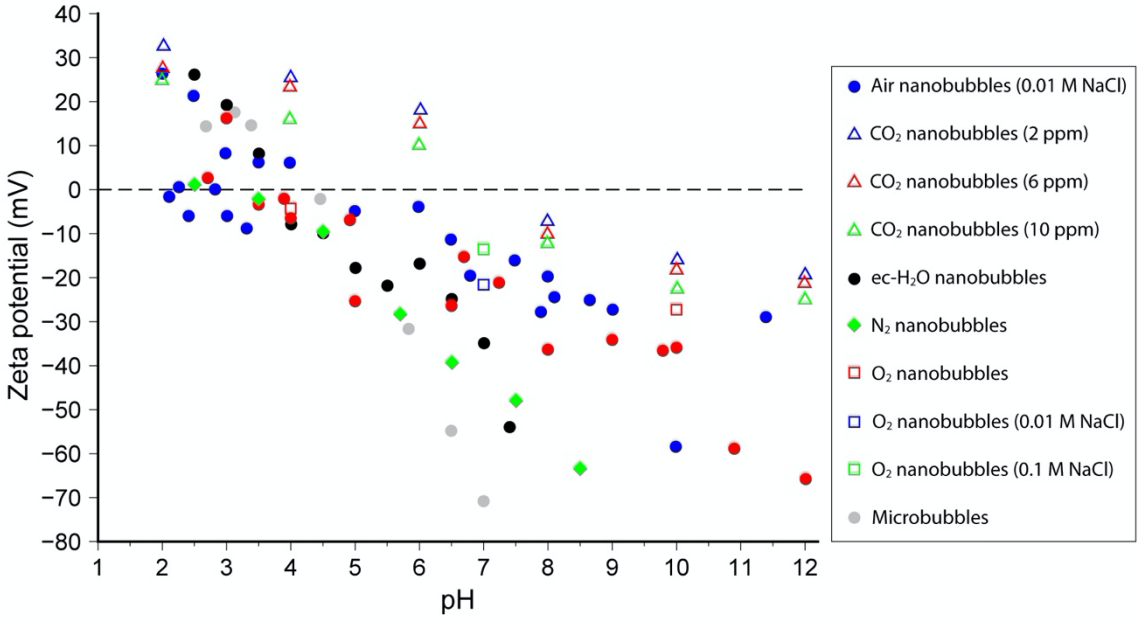

Fig. 2. Zeta potential of nanobubbles and microbubbles. Red solid circles: air nanobubbles in pure water [121,126]; Blue solid circles: air nanobubbles in 0.01 M NaCl solution [100,101]; Blue open triangles: nanobubbles with 2 ppm CO_2 [108]; Red open triangles: nanobubbles with 6 ppm CO_2 [108]; Green open triangles: nanobubbles with 10 ppm CO_2 [108]; Black solid circles: ec-H_2O nanobubbles [19]; Green solid diamonds: N_2 nanobubbles [125]; Red open squares: O_2 nanobubbles [127]; Blue open squares: O_2 nanobubbles in 0.01 M NaCl solution [127]; Green open squares: O_2 nanobubbles in 0.1 M NaCl solution [127]; Gray solid circle: microbubbles [124].

The zeta potential is commonly used to describe the stability of nanobubbles and their interactions with colloid particles, although several flaws are suspected in the use of the DLVO theory for nanobubbles. The electric double layer formed around a charged nanobubble consists of the Stern layer, an innermost region surrounding the bubble surface where ions are strongly attached, and the diffused layer where ions are loosely attached [133]. The zeta potential represents a potential at the imaginary boundary where ions within this boundary move with the bubble in the diffused layer. Thus, the zeta potential depends strongly on pH, ionic strength, temperature, and the concentration of additives [86]. For example, several studies have found a reduction in negative zeta potential with an increase in salinity (e.g., Figure 2) [127,133,134]. Yet, there is no experimental evidence on the presence of the Stern layer of nanobubbles. In contrast, the thickness of the double layer in an electrolyte solution is defined as the Debye length, solely dependent on the ionic strength. The reduction in the double layer thickness is found along with the reduction in zeta potential due to the increase in salinity [133]. More studies regarding the diffused double layer theory for nanobubbles are necessary to better understand the electric interactions of nanobubbles and other particles.

4. Nanobubbles as unique mitigation methods for corrosion and scaling

4.1. Nanobubbles as corrosion mitigation

Nanoscopic corrosion pathways have a significant influence on the corrosion behavior of carbon steel [135]. Real-time observations by Hayden et al. [136] have revealed that the localized corrosion of low-carbon steel initiates at the triple junction formed by an isolated cementite inclusion and two abutting ferrite grains. The localized corrosion is then advanced along with the electrochemically active interface of the two phases where a surface contact length has 100's of nanometers [136]. Thus, there are growing expectations for nanoscopic approaches to the effective mitigation of corrosion. Here, nanobubbles can be an environment-friendly, easy-to-use, and inexpensive additive agent by acting as a nanoscopic coating on the steel surfaces of the pipes and equipment in the geothermal system. Aikawa et al. [23] were the first to study the use of nanobubbles as a corrosion inhibitor by testing immersion corrosion of low-carbon steel in the acidic geothermal fluid (pH = 3.4–3.6, 75–85°C, SiO_2 = 860 mg/L) on-site a geothermal power plant in Kyushu area, Japan. The study performed weight loss measurements of the low-carbon steel coupons immersed in the untreated geothermal fluid (original geothermal fluid) and the geothermal fluid with continuous injection of the air-nanobubbles for 1 week, and analyzed the microstructure and chemical composition of the surfaces of immersed coupons. Their work showed that air-nanobubbles could inhibit the corrosion of low-carbon steels, with an inhibition efficiency of 20–50% for 7 days in the studied acidic geothermal fluid (Table 1).

The slip length may first decrease and the friction force on the steel wall may decrease, once a few nanobubbles are settled on the surface of steel [137]. With an increase in the surface coverage of nanobubbles, however, the slip length will increase (see Section 3). The slip length can be even larger in the acidic solution, due to higher hydrogen ion concentration leading to an increase in the absolute value of surface charge [138]. After further continuous injection of nanobubbles allowing that nanobubbles cover greater areas of the steel surface, the slip length further increases [94] with a lower drag of liquid flow at the interface. Also, the contact angle of nanobubbles on a rougher surface decreases [95,96] due to corrosion, leading to reduction of the friction and enhancement of wettability on the resulting rough steel surface. In the immersion test done by Aikawa et al. [23] that showed the inhibition effectiveness already in the first 24 hours of immersion in the acidic geothermal fluid, nanobubbles had already covered most of the steel surface or at least the sufficient area of the surface that could make a significant increase in the slip length within the first 24 hours. They also found that silica concentrations of the coupons immersed in the geothermal fluid with continuous injection of the air-nanobubbles for 2–7 days were slightly higher than those in the untreated geothermal fluid for respective time durations. As found by several studies [36,39–41], the formation of an initial layer of silica precipitation can also help to impede the underlying surface of pipe steel from further reacting with flowing geothermal fluid. Therefore, nanobubbles can act as a nanoscopic material in mitigating corrosion, by (i) increasing the slip length on the steel interface, (ii) behaving like the bubble

mattress covering most of the steel surface to isolate the steel surface from the geothermal fluid for the further reaction of corrosion and/or (iii) promoting a very small quantity of silica precipitates on the corrosive steel surface (Figure 3). Among these mechanisms of corrosion mitigation by nanobubbles, increasing the slip length and minimizing the surface exposure to the fluid (i and ii) would be the predominant mechanisms, because the inhibition effectiveness had already been seen in the first 24 hours of immersion where had least silica depositions [23]. The use of nanobubbles with higher number densities (e.g., 10^{10}–10^{11} bubbles per mL rather than a typical number density of 10^{8} bubbles per mL) may represent a better inhibition because it results in covering larger areas of the steel surface (Figure 3).

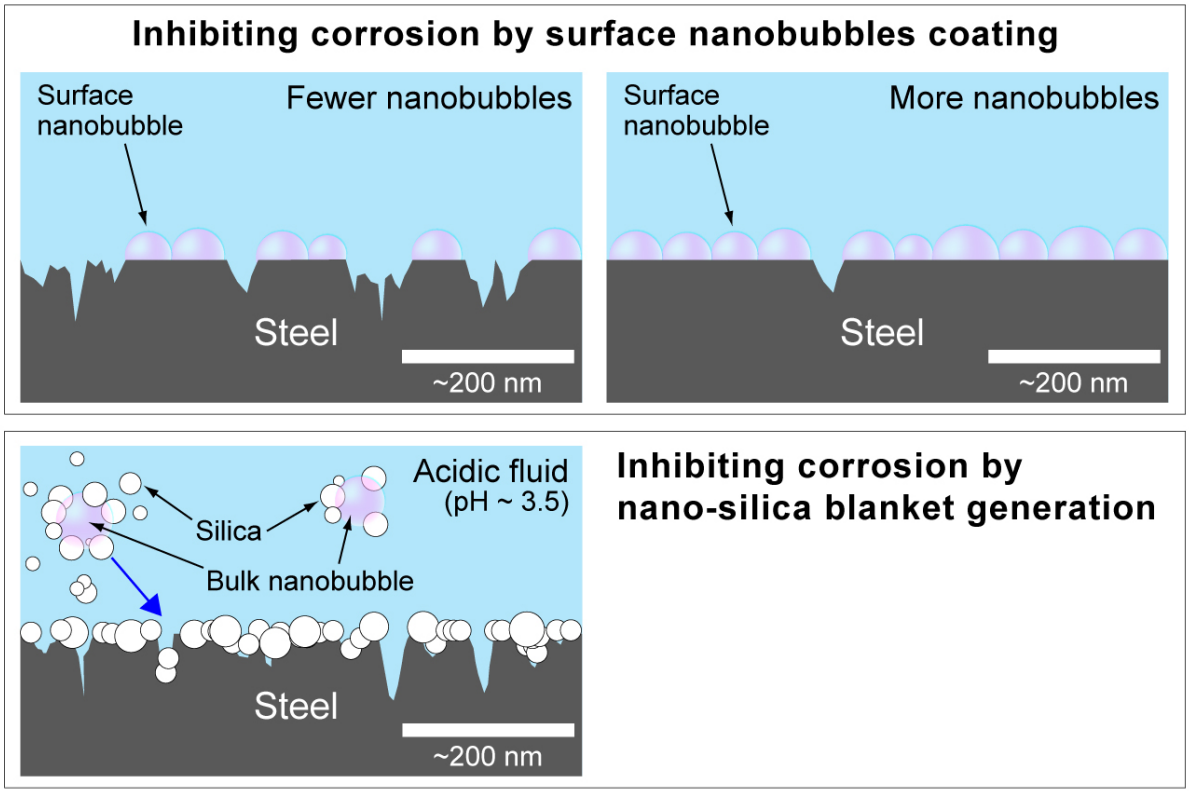

Fig. 3. Schematic illustration of roles of nanobubbles for inhibiting corrosion. Modified from Aikawa et al. [23].

This successful corrosion inhibition by adding air-nanobubbles might be counter-intuitive findings, because injecting air-nanobubbles in the geothermal fluid means entrapping more oxygen into the geothermal fluid which could intrusively accelerate the corrosion process. The nanobubbles generated by oxygen gases increase dissolved oxygen concentrations in water [139–141]. The nanobubbles generated by air were also possible to increase dissolved oxygen concentration in the geothermal water open to the air. The electrochemical corrosion potential of metals in high-temperature aqueous solution is known to increase with dissolved oxygen concentration [142]. As expected from the Pourbaix diagram [143], the increase in electrochemical corrosion potential is likely to lead

the corrosion process to the stability region of hematite (Fe_2O_3). The formation of semi-protective hematite on the passive film on the steel surface is then encouraged through oxidizing the outer surface of protective magnetite (Fe_3O_4), with the help of high dissolved oxygen concentration and the resulting elevation of electrochemical corrosion potential [144–146]. Therefore, the elevated dissolved oxygen concentration in the acidic geothermal water due to air-nanobubbles injection might also help mitigating corrosion [23].

Nanobubbles have not yet been proven to achieve an inhibition efficiency greater than 80% as compared with several high-performing chemical inhibitors (Table 1). With the help of stability of nanobubbles, however, nanobubbles are expected to be effective at higher temperatures and pressures, broader pH ranges, and for longer periods than any other reported methods (Table 1). Furthermore, the use of nanobubbles accepts any metal materials and the presence of fluid flow, while many of the examined methods are subject to either specific metal materials or flow properties. Therefore, the use of nanobubbles with higher number densities and selecting the right gases for generating nanobubbles (e.g., air, N_2, and O_2) with taking into account their feasible use will present the next studies that aim at enhancing the effectiveness of corrosion inhibition with different fluid chemistry.

4.2. Nanobubbles as inhibitor of scale formation

4.2.1. Nanobubbles as calcium carbonate scale inhibitor

It is well known that hydrodynamic properties, including flow rate, flow velocity, density, and viscosity, influence scale formation. Agglomeration of calcium carbonate increases with increasing residence time [147]. The roughness of the substrate surface also affects the nucleation and growth of calcium carbonate formation. The rate of nucleation of the calcium carbonate scale increases by an increase in surface roughness [148]. Additionally, geothermal fluid is known to precipitate scale when subjected to high shear stress [149]. The shear stress is linked to the slip length on the nanometer scale. By increasing the slip length on the metal surface, the fluid will have a shorter residence time. This will lead to less shear stress and thus, less opportunity to deposit calcium carbonates on the metal surface. Because the slip length can be significantly increased with the presence of nanobubbles on the hydrophobic surfaces (see Section 3), the surface nanobubbles may be able to increase the slip length by acting as a layer between the metal surface and the fluid, resulting in less scale precipitation on the surface.

The calcium carbonate scale normally occurs under neutral to alkali pH. Most data of zeta potential measured from natural calcites and carbonates indicate that the zeta potential of calcium carbonate is generally negative at pH of 6 to 12 and decreases with pH (Figure 4a) [150,151] but is independent of temperature [152]. Thus, nanobubbles may help disperse calcium carbonate particles to prevent their scale formation, given that the zeta potential of typical nanobubbles at pH > 7 is < −30 mV (Figure 2). However, the zeta potential of calcite is rather dependent on the calcium concentration (pCa) and decreases

linearly with higher pCa [151]. Therefore, nanobubbles may serve as a dispersant of calcium carbonate particles when their pCa is higher.

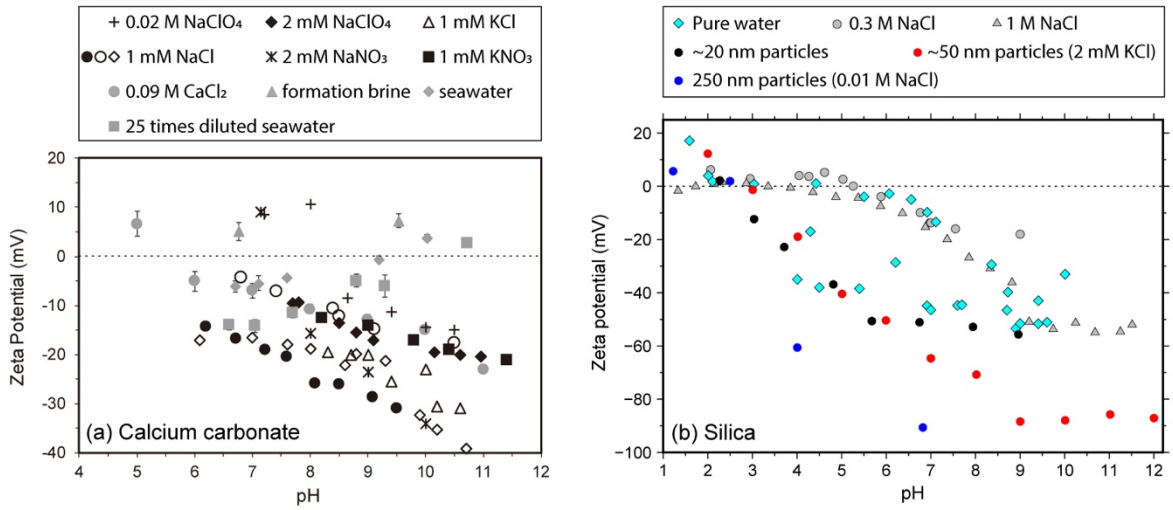

Fig. 4. (a) Zeta potential of natural calcium carbonate as a function of pH in different solutions. Modified from Al Mahrouqi et al. [151] and references therein. (b) Zeta potential of natural and synthetic silica as a function of pH. Cyan blue diamonds: pure water [158,159,162,163]; Solid gray circles: 0.3 M NaCl [159,163]; Solid gray triangles: 1 M NaCl solution [155]; Black solid circles: ~20 nm silica particles [157]; Red solid circles: ~50 nm silica particles in 2 mM KCl solution [156]; Blue solid circles: 250 nm silica particles in 0.01 M NaCl solution [161]. Note that magnitudes of zeta potential could be significantly larger with taking into account surface conductivity and Reynold number effects [160,164].

The formation of calcium carbonate scale represents complex processes involving crystallization and transport mechanisms. Crystals first form and then grow from a solution, while the condition of supersaturation is not necessarily sufficient for the crystallization of a solution. Nucleation of the calcium carbonate scale formation on the particle surfaces causes crystal growth when supersaturation exceeds a certain critical value. The subsequent scale formation occurs by the two crystallization ways, bulk crystallization and surface crystallization [8]. Bulk crystallization of calcium carbonate takes place when the crystal particles are formed in the bulk phase through homogenous nucleation, resulting in generating nuclei or seeds for the development of crystals and subsequent deposition. Here, bulk nanobubbles may be able to inhibit homogenous nucleation nanoscopically by dispersing calcium carbonate particles (Figure 5). Also, surface crystallization of calcium carbonate occurs along with heterogeneous nucleation and the lateral growth of the scale deposit on the metal surface. For inhibiting surface crystallization, we expect that surface nanobubbles may play a role as a dispersant to prevent heterogeneous nucleation of calcium carbonate crystals and/or avoid the lateral growth of deposit through generating a bubble mattress on the surface (Figure 5). Also, surface nanobubbles can simply play a role in thickening the fluid boundary layer on the metal surface, which can lengthen a path of

calcium carbonate colloids to the scaled surface. When most nanobubbles are present in bulk, their role for inhibiting homogenous nucleation and bulk crystallization is more dominant than inhibiting heterogeneous nucleation and surface crystallization. In contrast, when most nanobubbles are present as surface nanobubbles, they facilitate mitigating calcium carbonate by inhibiting heterogeneous nucleation than inhibiting homogenous nucleation. Furthermore, other than the role in covering the steel surface, the surface nanobubbles adsorbed onto the crystallographic faces of the calcite surface may play a similar role as the impurity-induced step pinning [153,154] that encourages to inhibit the calcite crystal growth. It yet remains open to understanding whether the effectiveness of nanobubbles on inhibiting the scale formation of calcium carbonate differs with their number density (from 10^6 to 10^{11} bubbles per mL), typical diameter (from a couple of 10's to several 100's of nanometers), and gas (e.g., air, O_2, N_2, and CO_2), which should be investigated in future studies.

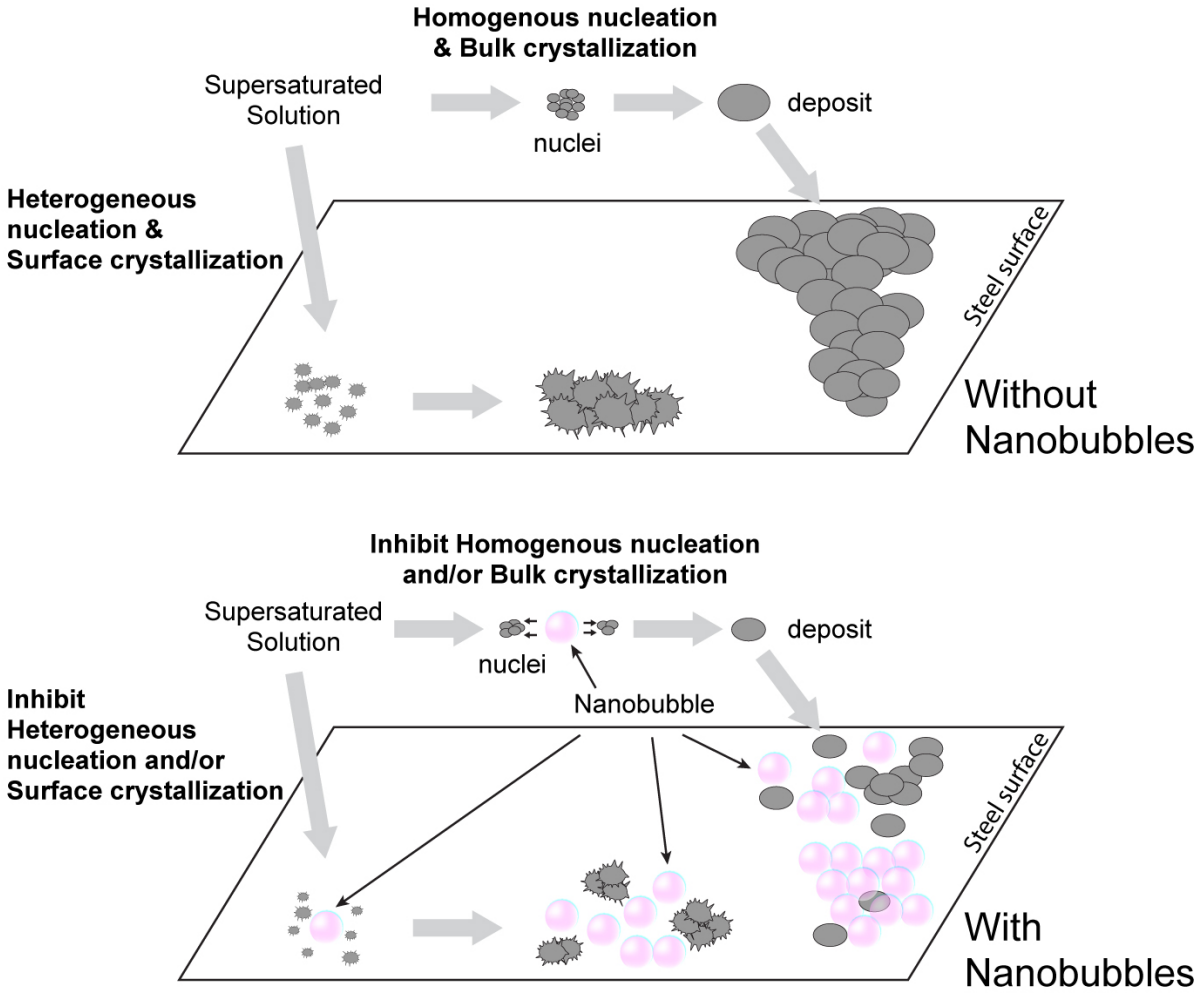

Figure 5: Schematic illustration of inhibiting $CaCO_3$ scale formation by using bulk and surface nanobubbles.

4.2.2. Nanobubbles as silica scale inhibitor

576 Zeta-potential measurements of silica colloids as a function of pH show that the
577 isoelectric point of silica nanoparticles is around pH 2 [155–158]. In a pH higher than 2 or 3,
578 the zeta potential of silica is generally negative and decreases with pH (Figure 4b) [155–
579 163], indicating that the silica surface is negatively charged and functionalized with $Si\text{-}O^-$
580 groups. Silica particles are generally stable at low pH, while the behavior of small particles is
581 more complex [165]. In the neutral solution with a pH greater than 5 or 6, both silica and
582 nanobubbles are negatively charged. Absolute values of zeta potentials of both silica and
583 nanobubbles are large enough to be able to inhibit silica scaling perhaps by stabilizing
584 particle-nanobubbles interactions. This may lead to inhibit silica polymerization and
585 consequent agglomeration of silica colloids (Figure 6), although the mechanism of how
586 nanobubbles inhibit polymerization remains a complex and open question (e.g., inhibiting
587 silicate anion growth, dehydration, and monomer condensation). The inhibition efficiencies
588 of agglomeration and polymerization are expected to be variable with the typical size,
589 number density, and gas species of nanobubbles.
590 On the other hand, in the acidic fluid environment, silica polymerization is delayed at
591 lower pH [166–168], suggesting monomeric silica favors in the deposition in the acidic
592 solution. Nanobubbles are generally positively charged in the acidic solutions of pH = 2.5–4.
593 (Figure 2). Absolute values of zeta potentials of silica and nanobubbles are equally small at a
594 pH of around 3 (Figures 2 & 4b). Thus, the nanobubble addition could electrochemically
595 adsorb and aggregate nano-silica particles in the acidic fluid at pH of ~2.5–4, perhaps by
596 forming “gas bridges” between silica particles [15,169]. This might make difficult to mitigate
597 nucleation of silica monomers and inhibit their succeeding growth on the metallic surface
598 (e.g. [23]).
599

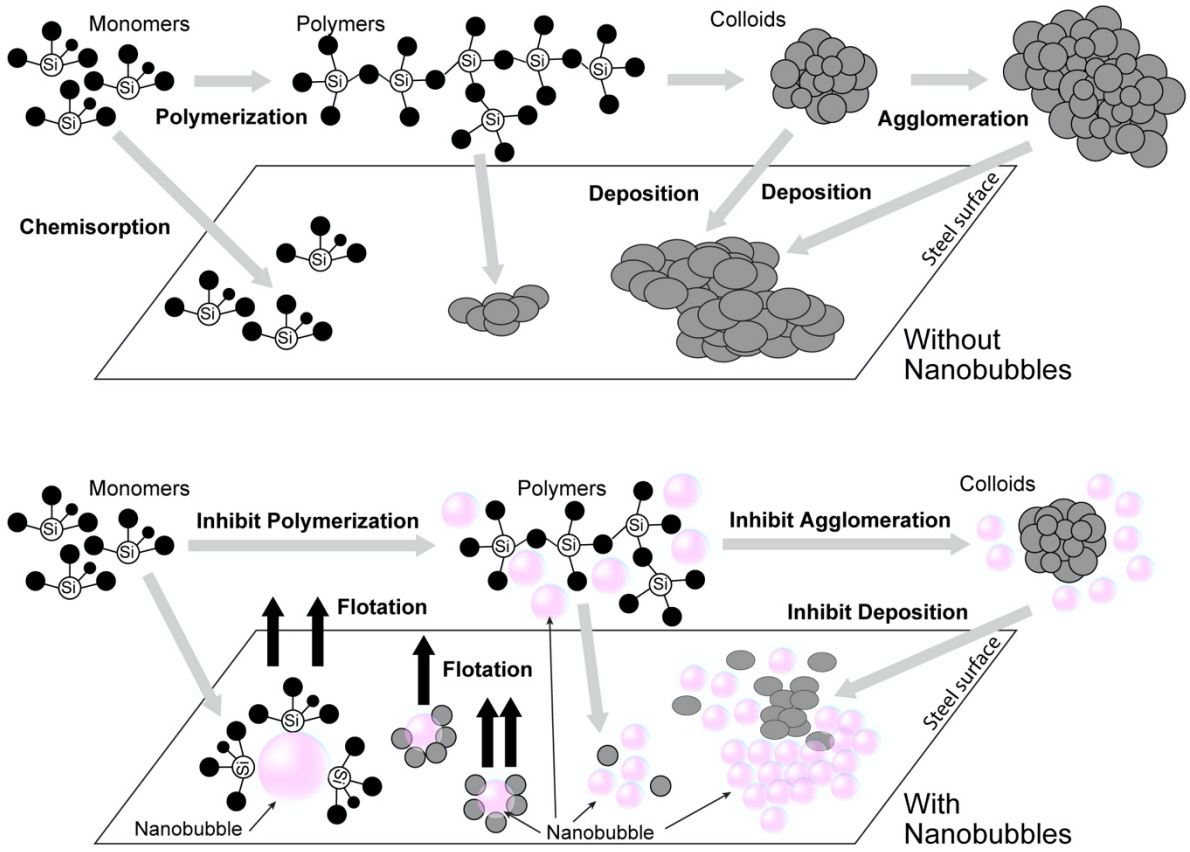

Figure 6: Schematic illustration of inhibiting silica scale formation by using bulk and surface nanobubbles.

Nevertheless, in the acidic environment where the magnitudes of zeta potential of both nanobubbles and silica are close to zero, nanobubbles may alternatively be beneficial to silica scale prevention by acting as a chemical-free means of enabling silica removal through the particle flotation [169]. The probability of particle collision P_c can be approximated to [170,171]:

$$P_c \propto \left(\frac{D_p}{D_b}\right)^2$$

where D_p and D_b are the diameters of the particle and the bubble, respectively. This suggests that the particle collision probability increases with larger particle size and smaller bubble size, indicating that nanobubbles experience more frequent collisions than microbubbles do. There is a strong attractive force between hydrophobic surfaces, which is caused in the presence of nanobubbles at the hydrophobic solid-liquid interface [172]. Nanobubbles can increase particle hydrophobicity [130]. The ratio of the total attachment force F_a and the total detachment force F_d can be approximated as [171]:

$$\frac{F_a}{F_d} \propto \frac{1 + D_p/D_b}{D_p^2}$$

which indicates that the ratio F_a/F_d decreases with larger silica particles D_p and larger bubbles D_b. Thus, as compared with larger bubbles, nanobubbles enhance the nanobubble-particle attachment probability while they reduce the detachment probability. The

attachment probability might be further enhanced in lower pH because the size of higher charged nanobubbles would be smaller in the acidic solution [101], although alternatively, lower pH might induce a lower number density of bubbles [121] leading to less attachment probability. The improvement on particles that are hard to float is more significant than on the particles that are easy to float. It is also known that nanobubbles can extend the size range of flotation of coarse particles to a lower limit of a few microns and an upper limit of 1 mm [173]. Therefore, bulk nanobubbles may tend to attach to the silica surface to prevent deposition by assisting flotation in the acidic solution (Figure 6).

As reviewed in the calcium carbonate scale, silica scale precipitation also increases with a longer fluid residence time and higher shear stress on the metal surface [174]. Chances of silica deposition increase when silica particles move slow enough to come to rest on and attach to the metal surface [175]. In addition, an early stage of silica precipitation is strongly influenced by the surface roughness of the substrate [176]. Thus, surface nanobubbles on the metal surface will help to mitigate silica scaling by not only playing as a coating material on the metal surface but also increasing the slip length and decreasing the shear rate on the surface. Moreover, surface nanobubbles can also play a role in thickening the fluid boundary layer on the metal surface, lengthening a path of silica colloids to the scaled surface. Furthermore, an extensive study of silica precipitation reaction based on stoichiometry and activities of the reactants derived a simple differential rate equation for silica precipitations [62]. The reaction rate is directly proportional to the interfacial area (A) between the solid and aqueous phases and inversely proportional to the mass of the aqueous solution (M) the silica is dissolving. Here nanobubbles can minimize the A/M ratio. Therefore, surface nanobubbles are expected to prevent a wide range of silica particles to physically prevent them from attaching to the surface probably independent of the electrochemical condition of the solution (Figure 6).

5. Conclusions and future studies of nanobubbles for geothermal applications

This paper has reviewed for the first time whether nanobubbles can mitigate corrosion and scale formation of calcium carbonate and silica in the geothermal fluid, based on theoretical views and experimental studies. Nanobubbles may not represent perfect inhibition effectiveness for corrosion and scaling of calcium carbonate and silica on the steel surface (e.g., the inhibition effectiveness for corrosion in the acidic geothermal fluid with air nanobubbles was up to 50%) as compared with several high-functional chemical inhibitors achieving the inhibition efficiency of 99%. However, nanobubbles have an edge on being chemically benign and their stabilities at high temperatures and pressures and broad ranges of pH, overcoming the limitations and disadvantages accommodated in most of the chemical inhibitors. We thus suggest nanobubbles can be a powerful "green" and inexpensive additive for inhibiting corrosion and scale formation. The mechanisms on how nanobubbles act as an inhibitor of corrosion and scaling may vary with their typical size (from a couple of 10's to several 100's of nanometers), gas species (e.g., air, O_2, N_2, and CO_2), and number density (from 10^6 to 10^{11} bubbles per mL), and different chemical conditions and fluid velocities of geothermal fluid, which should be investigated in the future studies.

One of the biggest challenges for utilizing nanobubbles we may face is the continuous generation of nanobubbles in the geothermal equipment for several months or a year. As compared with the ground applications studied in most of the previous inhibitor studies, the continuous generation of nanobubbles within long-buried pipes in the geothermal power plant may require installations of secure nanobubble generators within the pipes to ensure the inhibition of corrosion and scale formation during its operation. However, given the unique physicochemical properties of nanobubbles reviewed in the paper, we would suggest that the pipe surface could be modified to rather encourage the cavitation of flowing fluid. This allows the production of nanobubbles without installing nanobubble generators in equipment such as the pipe close to the separator because nanobubbles are generated by cavitation under high pressure, while control will be an issue with such a manipulated surface. Moreover, the pipes in geothermal plant infrastructure could be made more hydrophobic using different hydrophobic pipe materials to increase the slip length along pipe walls and decrease scale depositions with the help of nanobubbles. It should also be noted that nanobubbles may exist everywhere in nature, yet their presence has not been directly observed. Although more experiments, measurements, and observations are still necessary to examine these hypotheses, man-made and natural nanobubbles would be utilized as a "green" solution for geothermal problems.

Acknowledgments

We thank the two anonymous reviewers and the Associate Editor Prof. Sotirios Karellas for constructive comments that significantly improved our manuscript. We are also

grateful to S. Anzai for his valuable information and resource. A part of the topics in the paper was benefited from fruitful discussion with A. Aikawa, K. Tagomori, T. Kodama, A. Ueda, T. Yokoyama, K. Yonezu, and Y. Kiyota. This work is supported by the Frontiers in Engineering Research from Kyushu University (FY2020-2021) and JSPS KAKENHI Grant-in-Aid for Early-Career Scientists (JP21K14576).

Data Availability Statement

This work is done by compiling data from the existing relevant literature, and there is no additional data. The authors attest that all data for this study are included in the paper.

Funding Data

Frontiers in Engineering Research, Kyushu University (FY2020-2021)
JSPS KAKENHI Grant-in-Aid for Early-Career Scientists (JP21K14576)

Declaration of competing interest

The authors declare that they have no known competing financial interests or personal relationships that could have appeared to influence the work reported in this paper.

References

[1] Gallup DL. Production engineering in geothermal technology: A review. Geothermics 2009;38:326–34. https://doi.org/10.1016/j.geothermics.2009.03.001

[2] Nogara J, Zarrouk SJ. Corrosion in geothermal environment: Part 1: Fluids and their impact. Renew Sustain Energy Rev 2018;82:1333–46. https://doi.org/10.1016/j.rser.2017.06.098

[3] Nogara J, Zarrouk SJ. Corrosion in geothermal environment: Part 2: Metals and alloys. Renew Sustain Energy Rev 2018;82:1347–63. https://doi.org/10.1016/j.rser.2017.06.091

[4] Vallejo Vitaller A, Angst UM, Elsener, B. Laboratory tests simulating corrosion in geothermal power plants: influence of service conditions. Geotherm Energy 2020;8:9. https://doi.org/10.1186/s40517-020-00163-y

[5] Müller-Steinhagen H. Heat Exchanger Fouling: Mitigation and Cleaning Techniques. UK: Institution of Chemical Engineers; 2000.

[6] MacAdam J, Parsons SA. Calcium carbonate scale formation and control. Rev Environ Sci Biotechnol 2004;3:159–69. https://doi.org/10.1007/s11157-004-3849-1

[7] Alabi A, Chiesa M, Garlisi C, Palmisano G. Advances in anti-scale magnetic water treatment. Environ Sci Water Res Technol 2015;1:408–25. https://doi.org/10.1039/C5EW00052A

[8] Antony A, Low JH, Gray S, Childress AE, Le-Clech P, Leslie G. Scale formation and control in high pressure membrane water treatment: A review. J Membr Sci 2011;383:1–16. https://doi.org/10.1016/j.memsci.2011.08.054

[9] Corsi R. Scaling and corrosion in geothermal equipment: problems and preventive measures. Geothermics 1986;15:839–56. https://doi.org/10.1016/0375-6505(86)90097-0

[10] Mroczek E, Graham D, Siega C, Bacon L. Silica scaling in cooled silica saturated geothermal water: Comparison between Wairakei and Ohaaki geothermal fields, New Zealand. Geothermics 2017;69:145–52. https://doi.org/10.1016/j.geothermics.2017.05.006

[11] Okazaki T, Orii T, Ueda A, Ozawa A, Kuramitz H. Fiber Optic Sensor for Real-Time Sensing of Silica Scale Formation in Geothermal Water. Sci Rep 2017;7:3387. https://doi.org/10.1038/s41598-017-03530-1

[12] van den Heuvel DB, Gunnlaugsson E, Gunnarsson I, Stawski TM, Peacock CL, Benning LG. Understanding amorphous silica scaling under well-constrained conditions inside geothermal pipelines. Geothermics 2018;76:231–41. https://doi.org/10.1016/j.geothermics.2018.07.006

[13] Pambudi NA, Itoi R, Jalilinasrabady S, Gürtürk M. Sustainability of geothermal power plant combined with thermodynamic and silica scaling model. Geothermics 2018;71:108–17. https://doi.org/10.1016/j.geothermics.2017.09.003

[14] Alheshibri M, Qian J, Jehannin M, Craig VSJ. A History of Nanobubbles. Langmuir 2016;32:11086–100. https://doi.org/10.1021/acs.langmuir.6b02489

[15] Atkinson AJ, Apul OG, Schneider O, Garcia-Segura S, Westerhoff P. Nanobubble Technologies Offer Opportunities To Improve Water Treatment. Acc Chem Res 2019;52:1196–205. https://doi.org/10.1021/acs.accounts.8b00606

[16] Lohse D, Zhang X. Surface nanobubbles and nanodroplets. Rev Mod Phys 2015;87:981–1035. https://doi.org/10.1103/RevModPhys.87.981

[17] Agarwal A, Ng WJ, Liu Y. Principle and applications of microbubble and nanobubble technology for water treatment. Chemosphere 2011;84:1175–80. https://doi.org/10.1016/j.chemosphere.2011.05.054

[18] Temesgen T, Bui TT, Han M, Kim T-il, Park H. Micro and nanobubble technologies as a new horizon for water-treatment techniques: A review. Adv Colloid Interf Sci 2017;246:40–51. https://doi.org/10.1016/j.cis.2017.06.011

[19] Zhu J, An H, Alheshibri M, Liu L, Terpstra PMJ, Liu G, et al. Cleaning with Bulk Nanobubbles. Langmuir 2016;32:11203–11. https://doi.org/10.1021/acs.langmuir.6b01004

[20] Liu S-Y, Kundu P, Huang T-W, Chuang Y-J, Tseng F-G, Lu Y, et al. Quasi-2D liquid cell for high density hydrogen storage. Nano Energy 2017;31:218–24. https://doi.org/10.1016/j.nanoen.2016.11.017

[21] Liu S, Oshita S, Makino Y, Wang Q, Kawagoe Y, Uchida T. Oxidative Capacity of Nanobubbles and Its Effect on Seed Germination. ACS Sustain Chem Eng 2016;4:1347–53. https://doi.org/10.1021/acssuschemeng.5b01368

[22] Liu S, Oshita S, Kawabata S, Makino Y, Yoshimoto T. Identification of ROS Produced by Nanobubbles and Their Positive and Negative Effects on Vegetable Seed Germination. Langmuir 2016;32:11295–302. https://doi.org/10.1021/acs.langmuir.6b01621

[23] Aikawa A, Kioka A, Nakagawa M, Anzai S. Nanobubbles as corrosion inhibitor in acidic geothermal fluid. Geothermics 2021;89:101962. https://doi.org/10.1016/j.geothermics.2020.101962

[24] Sato N. Whitney Award Lecture: Toward a More Fundamental Understanding of Corrosion Processes. Corrosion 1989;45:354–68. https://doi.org/10.5006/1.3582030

[25] Tang Z. A review of corrosion inhibitors for rust preventative fluids. Curr Opin Solid State Mater Sci 2019;23:100759. https://doi.org/10.1016/j.cossms.2019.06.003

[26] Sun W, Liu Y, Li T, Cui S, Chen S, Yu Q, et al. Anti-corrosion of amphoteric metal enhanced by MAO/corrosion inhibitor composite in acid, alkaline and salt solution. J Colloid Interf Sci 2019;554:488–99. https://doi.org/10.1016/j.jcis.2019.07.035

[27] Bentiss F, Traisnel M, Lagrenee M. The substituted 1,3,4-oxadiazoles: a new class of corrosion inhibitors of mild steel in acidic media. Corros Sci 2000;42:127–46. https://doi.org/10.1016/S0010-938X(99)00049-9

[28] Shokry H, Yuasa M, Sekine I, Issa RM, El-baradie HY, Gomma GK. Corrosion inhibition of mild steel by schiff base compounds in various aqueous solutions: part 1. Corros Sci 1998;40:2173–86. https://doi.org/10.1016/S0010-938X(98)00102-4

[29] Finšgar M, Jackson J. Application of corrosion inhibitors for steels in acidic media for the oil and gas industry: A review. Corros Sci 2014;86:17–41. https://doi.org/10.1016/j.corsci.2014.04.044

[30] Chauhan DS, Quraishi MA, Wan Nik WB, Srivastava V. Triazines as a potential class of corrosion inhibitors: Present scenario, challenges and future perspectives. J Mol Liq 2021;321:114747. https://doi.org/10.1016/j.molliq.2020.114747

[31] El-Hajjaji F, Messali M, Martínez de Yuso MV, Rodríguez-Castellón E, Almutairi S, Bandosz TJ, et al. Effect of 1-(3-phenoxypropyl) pyridazin-1-ium bromide on steel corrosion inhibition in acidic medium. J Colloid Interf Sci 2019;541:418–24. https://doi.org/10.1016/j.jcis.2019.01.113

[32] Solomon MM, Umoren SA, Quraishi MA, Salman M. Myristic acid based imidazoline derivative as effective corrosion inhibitor for steel in 15% HCl medium. J Colloid Interf Sci 2019;551:47–60. https://doi.org/10.1016/j.jcis.2019.05.004

[33] Vasconcelos DCL, Carvalho JAN, Mantel M, Vasconcelos WL. Corrosion resistance of stainless steel coated with sol-gel silica. J Non-Cryst Solids 2000;273:135–9. https://doi.org/10.1016/S0022-3093(00)00155-1

[34] Sharma R, Barhai PK, Kumari N. Corrosion resistant behaviour of DLC films. Thin Solid Films 2008;516:5397–403. https://doi.org/10.1016/j.tsf.2007.07.099

[35] Nitta S, Kimura Y. Formation of SiO_2 thin film on SUS304 stainless steel by liquid phase deposition. J Soc Mater Sci Jpn 1994;43:1437–43. https://doi.org/10.2472/jsms.43.1437

[36] Ning C, Mingyan L, Weidong Z. Fouling and Corrosion Properties of SiO_2 Coatings on Copper in Geothermal Water. Ind Eng Chem Res 2012;51:6001–17. https://doi.org/10.1021/ie202091b

[37] Umoren SA, Solomon MM, Obot IB, Suleiman RK. A critical review on the recent studies on plant biomaterials as corrosion inhibitors for industrial materials. J Ind Eng Chem 2019;76:91–115. https://doi.org/10.1016/j.jiec.2019.03.057

[38] Ong G, Kasi R, Subramaniam R. A review on plant extracts as natural additives in coating applications. Prog Org Coat 2021;151:106091. https://doi.org/10.1016/j.porgcoat.2020.106091

[39] Mundhenk N, Huttenloch P, Sanjuan B, Kohl T, Steger H, Rorn R. Corrosion and scaling as interrelated phenomena in an operating geothermal power plant. Corros Sci 2013;70:17–28. https://doi.org/10.1016/j.corsci.2013.01.003

[40] Meier D, Gunnlaugsson E, Gunnarsson I, Jamtveit B, Peacock C, Benning L. Microstructural and chemical variation in silica-rich precipitates at the Hellisheiði geothermal power plant. Mineral Mag 2014;78:1381–9. https://doi.org/10.1180/minmag.2014.078.6.04

[41] van den Heuvel DB, Gunnlaugsson E, Benning LG. Passivation of metal surfaces against corrosion by silica scaling. Proceedings of the 41st Workshop on Geothermal Reservoir Engineering; 2016; Stanford, CA; 2016. SGP-TR-209.

[42] Sanada N, Kurata Y, Nanjo H, Ikeuchi J. Material damage in high velocity acidic fluids. GRC Trans 1995;19:359–63.

[43] Yanagisawa N, Masuda Y, Osato K, Sato M, Kasai K, Sakura K, et al. The Material Corrosion Test Using Small Loop System at Geothermal Power Plant in Japan. Proceedings of the 42nd Workshop on Geothermal Reservoir Engineering; 2017; Stanford, CA; 2017. SGP-TR-212.

[44] Andritsos N, Karabelas AJ. The Influence of Particulates on $CaCO_3$ Scale Formation. ASME J Heat Transfer 1999;121:225–7. https://doi.org/10.1115/1.2825951

[45] Cho YI, Fan C, Choi B-G. Use of electronic anti-fouling technology with filtration to prevent fouling in a heat exchanger. Int J Heat Mass Transf 1998;41:2961–6. https://doi.org/10.1016/S0017-9310(98)00011-8

[46] Dalas E. The effect of ultrasonic field on calcium carbonate scale formation. J Cryst Growth 2001;222:287–92. https://doi.org/10.1016/S0022-0248(00)00895-2

[47] Hartley AM, House WA, Callow ME, Leadbeater BSC. Coprecipitation of phosphate with calcite in the presence of photosynthesizing green algae. Water Res 1997;31:2261–8. https://doi.org/10.1016/S0043-1354(97)00103-6

[48] Hoch AR, Reddy MM, Aiken GR. Calcite crystal growth inhibition by humic substances with emphasis on hydrophobic acids from the Florida Everglades. Geochim Cosmochim Acta 2000;64:61–72. https://doi.org/10.1016/S0016-7037(99)00179-9

[49] Tang Y, Yang W, Yin X, Liu Y, Yin P, Wang J. Investigation of $CaCO_3$ scale inhibition by PAA, ATMP and PAPEMP. Desalination 2008;228:55–60. https://doi.org/10.1016/j.desal.2007.08.006

[50] Gopi SP, Subramanian VK. Polymorphism in CaCO3 – Effect of temperature under the influence of EDTA (di sodium salt). Desalination 2012;297:38–47. https://doi.org/10.1016/j.desal.2012.04.015

[51] Kiaei Z, Haghtalab A. Experimental study of using Ca-DTPMP nanoparticles in inhibition of $CaCO_3$ scaling in a bulk water process. Desalination 2014;338:84–92. https://doi.org/10.1016/j.desal.2014.01.027

[52] Martinod A, Euvrard M, Foissy A, Neville A. Progressing the understanding of chemical inhibition of mineral scale by green inhibitors. Desalination 2008;220:345–52. https://doi.org/10.1016/j.desal.2007.01.039

[53] Dietzsch M, Barz M, Schüler T, Klassen S, Schreiber M, Susewind M, et al. PAA-PAMPS Copolymers as an Efficient Tool to Control $CaCO_3$ Scale Formation. Langmuir 2013;29:3080–8. https://doi.org/10.1021/la4000044

[54] Sheikhi A, Li N, van de Ven TGM, Kakkar A. Macromolecule-based platforms for developing tailor-made formulations for scale inhibition. Environ Sci Water Res Technol 2016;2:71. https://doi.org/10.1039/C5EW00158G

[55] Stáhl G, Pátzay G, Weiser L, Kálmán E. Study of calcite scaling and corrosion processes in geothermal systems. Geothermics 2000;29:105–19. https://doi.org/10.1016/S0375-6505(99)00052-8

[56] Thomas DM, Gudmundsson JS. Advances in the study of solids deposition in geothermal systems. Geothermics 1989;18:5–15. https://doi.org/10.1016/0375-6505(89)90004-7

[57] Förster M, Bohnet M. Influence of the interfacial free energy crystal/heat transfer surface on the induction period during fouling. Int J Therm Sci 1999;38:944–54. https://doi.org/10.1016/S1290-0729(99)00102-7

[58] Zhao Q, Liu Y, Wang C, Wang S, Müller-Steinhagen H. Effect of surface free energy on the adhesion of biofouling and crystalline fouling. Chem Eng Sci 2005;60:4858–65. https://doi.org/10.1016/j.ces.2005.04.006

[59] Wang Y, Wang L-l, Liu M-y. Antifouling and enhancing pool boiling by TiO_2 coating surface in nanometer scale thickness. AIChE J 2007;53:3062–76. https://doi.org/10.1002/aic.11345

[60] Fournier RO, Rowe JJ. Estimation of underground temperatures from the silica content of water from hot springs and wet-steam wells. Am J Sci 1966;264:685–97. https://doi.org/10.2475/ajs.264.9.685

[61] Gunnarsson I, Arnórsson S. Impact of silica scaling on the efficiency of heat extraction from high-temperature geothermal fluids. Geothermics 2005;34:321–9. https://doi.org/10.1016/j.geothermics.2005.02.002

[62] Rimstidt JD, Barnes HL. The kinetics of silica-water reactions. Geochim Cosmochim Acta 1980;44:1683–99. https://doi.org/10.1016/0016-7037(80)90220-3

[63] Iler RK. The Chemistry of Silica: Solubility, Polymerization, Colloid and Surface Properties, and Biochemistry. New York: John Wiley & Sons; 1979.

[64] Greenberg SA, Sinclair D. The Polymerization of Silicic Acid. J Phys Chem 1955;59:435–40. https://doi.org/10.1021/j150527a014

[65] Shimada K, Tarutani T. The Kinetics of the Polymerization of Silicic Acid. Bull Chem Soc Jpn 1980;53:3488–91. https://doi.org/10.1246/bcsj.53.3488

[66] Zuhl RW, Amjad Z. Solution Chemistry Impact on Silica Polymerization by Inhibitors. In: Amjad Z, editor. Mineral Scales in Biological and Industrial Systems. Boca Raton: CRC Press; 2013. p. 173–200.

[67] Yokoyama T, Takahashi Y, Yamanaka C, Tarutani T. Effect of aluminium on the polymerization silicic acid in aqueous solution and the deposition of silica. Geothermics 1989;18:321–6. https://doi.org/10.1016/0375-6505(89)90042-4

[68] Yokoyama T, Takahashi Y, Tarutani T. Retarding and accelerating effects of aluminum on the growth of polysilicic acid particles. J Colloid Interf Sci 1991;141:559–63. https://doi.org/10.1016/0021-9797(91)90352-9

[69] Yokoyama T, Sato Y, Maeda Y, Tarutani T, Itoi R. Siliceous deposits formed from geothermal water I. The major constituents and the existing states of iron and aluminium. Geochem J 1993;27:375–84. https://doi.org/10.2343/geochemj.27.375

[70] Manceau A, Ildefonse Ph, Hazemann J-L, Flank AM, Gallup D. Crystal Chemistry of Hydrous Iron Silicate Scale Deposits at the Salton Sea Geothermal Field. Clays Clay Miner 1995;43:304–17. https://doi.org/10.1346/CCMN.1995.0430305

[71] Pokrovski GS, Schott J, Harrichoury J-C, Sergeyev AS. The stability of aluminum silicate complexes in acidic solutions from 25 to 150°C. Geochim Cosmochim Acta 1996;60:2495–501. https://doi.org/10.1016/0016-7037(96)00123-8

[72] Gallup DL. Aluminum silicate scale formation and inhibition (2): scale solubilities and laboratory and field inhibition tests. Geothermics 1998;27:485–501. https://doi.org/10.1016/S0375-6505(98)00024-8

[73] Gallup DL. Brine pH Modification Scale Control Technology. 2. A Review. GRC Trans 2011;35:609–14.

[74] Hirowatari K. Scale prevention method by brine acidification with biochemical reactors. Geothermics 1996;25:259–70. https://doi.org/10.1016/0375-6505(95)00043-7

[75] Masunaga S, Yonezu K, Etou M, Kawamoto D, Yamamoto Y, Kiyota Y, et al. Effect of polyacrylic acid on polymerization and deposition of silicic acid in geothermal water: A case study at Takigami geothermal power plant, Oita Prefecture. J Geotherm Res Soc Jpn 2017;39:181–9. https://doi.org/10.11367/grsj.39.181

[76] Ueda A, Kato K, Mogi K, Mroczek E, Thain IA. Silica removal from Mokai, New Zealand, geothermal brine by treatment with lime and a cationic precipitant. Geothermics 2003;32:47–61. https://doi.org/10.1016/S0375-6505(02)00050-0

[77] Demadis KD, Stathoulopoulou A. Solubility Enhancement of Silicate with Polyamine/Polyammonium Cationic Macromolecules: Relevance to Silica-Laden Process Waters. Ind Eng Chem Res 2006;45:4436–40. https://doi.org/10.1021/ie0602254

[78] Ketsetzi A, Stathoulopoulou A, Demadis KD. Being “green” in chemical water treatment technologies: issues, challenges and developments. Desalination 2008;223:487–93. https://doi.org/10.1016/j.desal.2007.01.230

[79] Hanajima E, Ueda A. Recovery of oversaturated silica from Takigami and Sumikawa geothermal brines with cationic polymer flocculants to prevent silica scale deposition. Geothermics 2017;70:271–80. https://doi.org/10.1016/j.geothermics.2017.07.001

[80] Bush JA, Vanneste J, Gustafson EM, Waechter CA, Jassby D, Turchi CS, et al. Prevention and management of silica scaling in membrane distillation using pH adjustment. J Membr Sci 2018;554:366–77. https://doi.org/10.1016/j.memsci.2018.02.059

[81] Batis G, Kouloumbi N, Kotsakou K. Corrosion and protection of carbon steel in low enthalpy geothermal fluids. The case of Sousaki in Greece. Geothermics 1997;26:65–82. https://doi.org/10.1016/S0375-6505(96)00030-2

[82] Sugama T, Webster R, Reams W, Gawlik K. High-performance polymer coatings for carbon steel heat exchanger tubes in geothermal environments. J Mater Sci 2000;35:2145–54. https://doi.org/10.1023/A:1004754204893

[83] Sugama T, Elling D, Gawlik K. Poly(phenylenesulfide)-based coatings for carbon steel heat exchanger tubes in geothermal environments. J Mater Sci 2002;37:4871–80. https://doi.org/10.1023/A:1020806012202

[84] Sugama T, Gawlik K. Self-repairing poly(phenylenesulfide) coatings in hydrothermal environments at 200°C. Mater Lett 2003;57:4282–90. https://doi.org/10.1016/S0167-577X(03)00304-5

[85] Ishida N, Inoue T, Miyahara M, Higashitani K. Nano Bubbles on a Hydrophobic Surface in Water Observed by Tapping-Mode Atomic Force Microscopy. Langmuir 2000;16:6377–80. https://doi.org/10.1021/la000219r

[86] Ruckenstein E. Nanodispersions of bubbles and oil drops in water. Colloids Surf A Physicochem Eng Asp 2013;423:112–4. https://doi.org/10.1016/j.colsurfa.2013.01.056

[87] Ohgaki K, Khanh NQ, Joden Y, Tsuji A, Nakagawa T. Physicochemical approach to nanobubble solutions. Chem Eng Sci 2010;65:1296–300. https://doi.org/10.1016/j.ces.2009.10.003

[88] Etchepare R, Oliveira H, Nicknig M, Azevedo A, Rubio J. Nanobubbles: Generation using a multiphase pump, properties and features in flotation. Miner Eng 2017;112:19–26. https://doi.org/10.1016/j.mineng.2017.06.020

[89] Michailidi ED, Bomis G, Varoutoglou A, Kyzas GZ, Mitrikas G, Mitropoulos ACh, et al. Bulk nanobubbles: Production and investigation of their formation/stability mechanism. J Colloid Interf Sci 2020;564:371–80. https://doi.org/10.1016/j.jcis.2019.12.093

[90] Weijs JH, Lohse D. Why Surface Nanobubbles Live for Hours. Phys Rev Lett 2013;110:054501. https://doi.org/10.1103/PhysRevLett.110.054501

[91] Zhang XH, Maeda N, Craig VSJ. Physical Properties of Nanobubbles on Hydrophobic Surfaces in Water and Aqueous Solutions. Langmuir 2006;22:5025–35. https://doi.org/10.1021/la0601814

[92] Lauga E, Stone HA. Effective slip in pressure-driven Stokes flow. J Fluid Mech 2003;489:55–77. https://doi.org/10.1017/S0022112003004695

[93] Niavarani A, Priezjev NV. Modeling the combined effect of surface roughness and shear rate on slip flow of simple fluids. Phys Rev E 2010;81:011606. https://doi.org/10.1103/PhysRevE.81.011606

[94] Wang Y, Bhushan B. Boundary slip and nanobubbles study in micro/nanofluidics using atomic force microscopy. Soft Matter 2010;629–66. https://doi.org/10.1039/B917017K

[95] Yen T-H. Effects of wettability and interfacial nanobubbles on flow through structured nanochannels: an investigation of molecular dynamics. Mol Phys 2015;113:3783–95. https://doi.org/10.1080/00268976.2015.1062928

[96] Li D, Jing D, Pan Y, Bhushan B, Zhao X. Study of the Relationship between Boundary Slip and Nanobubbles on a Smooth Hydrophobic Surface. Langmuir 2016;32:11287–94. https://doi.org/10.1021/acs.langmuir.6b02877

[97] Zhang X, Lhuissier H, Sun C, Lohse D. Surface Nanobubbles Nucleate Microdroplets. Phys Rev Lett 2014;112:144503. https://doi.org/10.1103/PhysRevLett.112.144503

[98] Borkent BM, Dammer SM, Schönherr H, Julius Vancso G, Lohse D. Superstability of Surface Nanobubbles. Phys Rev Lett 2007;98:204502. https://doi.org/10.1103/PhysRevLett.98.204502

[99] Kim JY, Song MG, Kim JD. Zeta Potential of Nanobubbles Generated by Ultrasonication in Aqueous Alkyl Polyglycoside Solutions. J Colloid Interf Sci 2000;223:285–91. https://doi.org/10.1006/jcis.1999.6663

[100] Najafi AS, Drelich J, Yeung A, Xu Z, Masliyah J. A novel method of measuring electrophoretic mobility of gas bubbles. J Colloid Interf Sci 2007;308:344–50. https://doi.org/10.1016/j.jcis.2007.01.014

[101] Calgaroto S, Wilberg KQ, Rubio J. On the nanobubbles interfacial properties and future applications in flotation. Miner Eng 2014;60:33–40. http://dx.doi.org/10.1016/j.mineng.2014.02.002

[102] Chen Q, Wiedenroth HS, German SR, White HS. Electrochemical Nucleation of Stable N2 Nanobubbles at Pt Nanoelectrodes. J Am Chem Soc 2015;137:12064–9. https://doi.org/10.1021/jacs.5b07147

[103] Calgaroto S, Azevedo A, Rubio J. Separation of amine-insoluble species by flotation with nano and microbubbles. Miner Eng 2016;89:24–9. https://doi.org/10.1016/j.mineng.2016.01.006

[104] Eklund F, Swenson J. Stable Air Nanobubbles in Water: the Importance of Organic Contaminants. Langmuir 2018;34:11003–9. https://doi.org/10.1021/acs.langmuir.8b01724

[105] Yasui K. Acoustic Cavitation and Bubble Dynamics. 1st ed. Cham, Switzerland: Springer International Publishing; 2018. https://doi.org/10.1007/978-3-319-68237-2

[106] Gogate PR, Pandit AB. A review and assessment of hydrodynamic cavitation as a technology for the future. Ultrason Sonochem 2005;12:21–7. https://doi.org/10.1016/j.ultsonch.2004.03.007

[107] Hielscher T. Ultrasonic Production of Nano-size Dispersions and Emulsions. arXiv:0708.1831 [Preprint]. 2007. Available from: https://arxiv.org/abs/0708.1831

[108] Fan M, Tao D, Honaker R, Luo Z. Nanobubble generation and its applications in froth flotation (part I): nanobubble generation and its effects on properties of microbubble and millimeter scale bubble solutions. Min Sci Tech 2010;20:1–19. https://doi.org/10.1016/S1674-5264(09)60154-X

[109] Tomita Y, Shima A. High-Speed Photographic Observations of Laser-Induced Cavitation Bubbles in Water. Acta Acust United Acust 1990;71:161–71.

[110] Ahmed AKA, Sun C, Hua L, Zhang Z, Zhang Y, Zhang W, et al. Generation of nanobubbles by ceramic membrane filters: The dependence of bubble size and zeta potential on surface coating, pore size and injected gas pressure. Chemosphere 2018;203:327–35. https://doi.org/10.1016/j.chemosphere.2018.03.157

[111] Kukizaki M, Goto M. Size control of nanobubbles generated from Shirasu-porous-glass (SPG) membranes. J Membr Sci 2006;281:386–96. https://doi.org/10.1016/j.memsci.2006.04.007

[112] Tabeling P. Introduction to Microfluidics. UK: Oxford University Press; 2005.
[113] Vinogradova OI, Yakubov GE. Dynamic Effects on Force Measurements. 2. Lubrication and the Atomic Force Microscope. Langmuir 2003;19:1227–34. https://doi.org/10.1021/la026419f
[114] Cottin-Bizonne C, Cross B, Steinberger A, Charlaix E. Boundary Slip on Smooth Hydrophobic Surfaces: Intrinsic Effects and Possible Artifacts. Phys Res Lett 2005;94:056102. https://doi.org/10.1103/PhysRevLett.94.056102
[115] Joly L, Ybert C, Bocquet, L. Probing the Nanohydrodynamics at Liquid-Solid Interfaces Using Thermal Motion. Phys Rev Lett 2006;96:046101. https://doi.org/10.1103/PhysRevLett.96.046101
[116] Vinogradova OI, Koynov K, Best A, Feuillebois F. Direct Measurements of Hydrophobic Slippage Using Double-Focus Fluorescence Cross-Correlation. Phys Rev Lett 2009;102:118302. https://doi.org/10.1103/PhysRevLett.102.118302
[117] Rothstein JP. Slip on Superhydrophobic Surfaces. Annu Rev Fluid Mech 2010;42:89–109. https://doi.org/10.1146/annurev-fluid-121108-145558
[118] Ramisetti SB, Borg MK, Lockerby DA, Reese JM. Liquid slip over gas nanofilms. Phys Rev Fluid 2017;2:084003. https://doi.org/10.1103/PhysRevFluids.2.084003
[119] Hyväluoma J, Kunert C, Harting J. Simulations of slip flow on nanobubble-laden surfaces. J Phys Condens Matter 2011;23:184106. https://doi.org/10.1088/0953-8984/23/18/184106
[120] Marinova KG, Alargova RG, Denkov ND, Velev OD, Petsev DN, Ivanov IB, et al. Charging of Oil-Water Interfaces Due to Spontaneous Adsorption of Hydroxyl Ions. Langmuir 1996;12:2045–51. https://doi.org/10.1021/la950928i
[121] Nirmalkar N, Pacek AW, Barigou M. Interpreting the interfacial and colloidal stability of bulk nanobubbles. Soft Matter 2018;14:9643. https://doi.org/10.1039/C8SM01949E
[122] Trefalt G, Borkovec, M. Overview of DLVO theory. Laboratory of colloid and surface chemistry [Internet]. Switzerland: University of Geneva; 2014. Available from http://www.colloid.ch/dlvo
[123] Spanos N, Klepetsanis PG, Koutsoukos PG. Calculation of Zeta-Potentials From Electrokinetic Data. In: Hubbard AT, editor. Encyclopedia of Surface and Colloid Science. UK: CRC Press; 2002. p. 829–45.
[124] Takahashi M. ζ Potential of Microbubbles in Aqueous Solutions: Electrical Properties of the Gas-Water Interface. J Phys Chem B 2005;109:21858–64. https://doi.org/10.1021/jp0445270
[125] Wang Q, Zhao H, Qi N, Qin Y, Zhang X, Li Y. Generation and Stability of Size-Adjustable Bulk Nanobubbles Based on Periodic Pressure Change. Sci Rep 2019;9:1118. https://doi.org/10.1038/s41598-018-38066-5
[126] Zhou W, Niu J, Xiao W, Ou L. Adsorption of bulk nanobubbles on the chemically surface-modified muscovite minerals. Ultrason Sonochem 2019;51:31–9. https://doi.org/10.1016/j.ultsonch.2018.10.021

[127] Zhang H, Guo Z, Zhang X. Surface enrichment of ions leads to the stability of bulk nanobubbles. Soft Matter 2020;16:5470–7. https://doi.org/10.1039/D0SM00116C
[128] Kelsall GH, Tang S, Yurdakul S, Smith AL. Electrophoretic behaviour of bubbles in aqueous electrolytes. J Chem Soc Faraday Trans 1996;92:3887–93. https://doi.org/10.1039/FT9969203887
[129] Beattie JK, Djerdjev AM, Warr GG. The surface of neat water is basic. Faraday Discuss 2008;141:31–9. https://doi.org/10.1039/B805266B
[130] Fan M, Tao D, Honaker R, Luo Z. Nanobubble generation and its applications in froth flotation (part II): fundamental study and theoretical analysis. Min Sci Tech 2010;20:159–77. https://doi.org/10.1016/S1674-5264(09)60179-4
[131] Calgaroto S, Azevedo A, Rubio J. Flotation of quartz particles assisted by nanobubbles. Int J Miner Process 2015;137:64–70. https://doi.org/10.1016/j.minpro.2015.02.010
[132] Azevedo A, Etchepare R, Calgaroto S, Rubio J. Aqueous dispersions of nanobubbles: Generation, properties and features. Miner Eng 2016;94:29–37. https://doi.org/10.1016/j.mineng.2016.05.001
[133] Meegoda JN, Hewage SA, Batagoda JH. Application of the Diffused Double Layer Theory to Nanobubbles. Langmuir 2019;35:12100–12. https://doi.org/10.1021/acs.langmuir.9b01443
[134] Uchida T, Liu S, Enari M, Oshita S, Yamazaki K, Gohara, K. Effect of NaCl on the Lifetime of Micro- and Nanobubbles. Nanomaterials 2016;6:31. https://doi.org/10.3390/nano6020031
[135] Dwivedi D, Lepková K, Becker T. Carbon steel corrosion: a review of key surface properties and characterization methods. RSC Adv 2017;7:4580–610. https://doi.org/10.1039/C6RA25094G
[136] Hayden SC, Chisholm C, Grudt RO, Aguiar JA, Mook WM, Kotula PG, et al. Localized corrosion of low-carbon steel at the nanoscale. npj Mater Degrad 2019;3:17. https://doi.org/10.1038/s41529-019-0078-1
[137] Maali A, Bhushan B. Nanobubbles and their role in slip and drag. J Phys Condens Matter 2013;25:184003. https://doi.org/10.1088/0953-8984/25/18/184003
[138] Li Y, Bhushan B. The effect of surface charge on the boundary slip of various oleophilic/phobic surfaces immersed in liquid. Soft Matter 2015;11:7680–95. https://doi.org/10.1039/C5SM00763A
[139] Ushikubo FY, Furukawa T, Nakagawa R, Enari M, Makino Y, Kawagoe Y, et al. Evidence of the existence and the stability of nano-bubbles in water. Colloids Surf A Physicochem Eng Asp 2010;361:31–7. https://doi.org/10.1016/j.colsurfa.2010.03.005
[140] Ebina K, Shi K, Hirao M, Hashimoto J, Kawato Y, Kaneshiro S, et al. Oxygen and Air Nanobubble Water Solution Promote the Growth of Plants, Fishes, and Mice. PLOS ONE 2013;8(6):e65339. https://doi.org/10.1371/journal.pone.0065339
[141] Liu Y, Zhou Y, Wang T, Pan J, Zhou B, Muhammad T, et al. Micro-nano bubble water oxygation: Synergistically improving irrigation water use efficiency, crop yield and quality. J Clean Prod 2019;222:835–43. https://doi.org/10.1016/j.jclepro.2019.02.208

[142] Kim Y-J, Andresen PL. Data Quality, Issues, and Guidelines for Electrochemical Corrosion Potential Measurement in High-Temperature Water. Corrosion 2003;59:584–96. https://doi.org/10.5006/1.3277589

[143] Beverskog B, Puigdomenech I. Revised pourbaix diagrams for iron at 25–300°C. Corros Sci 1996;38:2121–35. https://doi.org/10.1016/S0010-938X(96)00067-4

[144] Kumai CS, Devine TM. Influence of Oxygen Concentration of 288°C Water and Alloy Composition on the Films Formed on Fe-Ni-Cr Alloys. Corrosion 2007;63:1101–13. https://doi.org/10.5006/1.3278328

[145] Kuang W, Wu X, Han E-H. Influence of dissolved oxygen concentration on the oxide film formed on 304 stainless steel in high temperature water. Corros Sci 2012;63:259–66. https://doi.org/10.1016/j.corsci.2012.06.007

[146] Wang S, Yin X, Zhang H, Liu D, Dun N. Coupling Effects of pH and Dissolved Oxygen on the Corrosion Behavior and Mechanism of X80 Steel in Acidic Soil Simulated Solution. Materials 2019;12:3175. https://doi.org/10.3390/ma12193175

[147] Zhu G, Li H, Li S, Hou X, Xu D, Lin R, et al. Crystallization behavior and kinetics of calcium carbonate in highly alkaline and supersaturated system. J Cryst Growth 2015;428:16–23. https://doi.org/10.1016/j.jcrysgro.2015.07.009

[148] Gunn DJ. Effect of surface roughness on the nucleation and growth of calcium sulphate on metal surfaces. J Cryst Growth 1980;50:533–7. https://doi.org/10.1016/0022-0248(80)90104-9

[149] Hewett JN, Sellier M. Modelling ripple morphodynamics driven by colloidal deposition. Comput Fluids 2018;163:54–67. https://doi.org/10.1016/j.compfluid.2017.12.017

[150] Alroudhan A, Vinogradov J, Jackson MD. Zeta potential of intact natural limestone: Impact of potential-determining ions Ca, Mg and SO_4. Colloid Surf A Physicochem Eng Asp 2016;493:83–98. https://doi.org/10.1016/j.colsurfa.2015.11.068

[151] Al Mahrouqi D, Vinogradov J, Jackson MD. Zeta potential of artificial and natural calcite in aqueous solution. Adv Colloid Interf Sci 2017;240:60–76. https://doi.org/10.1016/j.cis.2016.12.006

[152] Al Mahrouqi D, Vinogradov J, Jackson MD. Temperature dependence of the zeta potential in intact natural carbonates. Geophys Res Lett 2016;43:11578–87. https://doi.org/10.1002/2016GL071151

[153] Sangwal K. Effects of impurities on crystal growth processes. Prog Cryst Growth Charact Mater 1996;32:3–43. https://doi.org/10.1016/0960-8974(96)00008-3

[154] Miura H. Phase-Field Modeling of Step Dynamics on Growing Crystal Surface: Step Pinning Induced by Impurities. Cryst Growth Des 2015;15:4142–8. https://doi.org/10.1021/acs.cgd.5b00762

[155] Xu P, Wang H, Tong R, Du Q, Zhong W. Preparation and morphology of SiO_2/PMMA nanohybrids by microemulsion polymerization. Colloid Polym Sci 2006;284:755–62. https://doi.org/10.1007/s00396-005-1428-9

[156] Alkhammash HI, Li N, Berthier R, de Planque MRR. Native silica nanoparticles are powerful membrane disruptors. Phys Chem Chem Phys 2015;17:15547–60. https://doi.org/10.1039/C4CP05882H

[157] Mandel K, Straßer M, Granath T, Dembski S, Sextl G. Surfactant free superparamagnetic iron oxide nanoparticles for stable ferrofluids in physiological solutions. Chem Commun 2015;51:2863–6. https://doi.org/10.1039/C4CC09277E

[158] Wang X, Shi L, Zhang J, Cheng J, Wang X. Self-assembly fabrication, microstructures and antibacterial performance of layer-structured montmorillonite nanocomposites with cationic silica nanoparticles. RSC Adv 2017;7:31502–11. https://doi.org/10.1039/C7RA04353H

[159] Bai S, Urabe S, Okaue Y, Yokoyama, T. Acceleration effect of sulfate ion on the dissolution of amorphous silica. J Colloid Interf Sci 2009;331:551–4. https://doi.org/10.1016/j.jcis.2008.11.076

[160] Leroy P, Devau N, Revil A, Bizi M. Influence of surface conductivity on the apparent zeta potential of amorphous silica nanoparticles. J Colloid Interf Sci 2013;410:81–93. https://doi.org/10.1016/j.jcis.2013.08.012

[161] Savaji KV, Niitsoo O, Couzis A. Influence of particle/solid surface zeta potential on particle adsorption kinetics. J Colloid Interf Sci 2014;431:165–75. https://doi.org/10.1016/j.jcis.2014.05.030

[162] Sikora A, Bartczak D, Geißler D, Kestens V, Roebben G, Ramaye Y, et al. A systematic comparison of different techniques to determine the zeta potential of silica nanoparticles in biological medium. Anal Methods 2015;7:9835–43. https://doi.org/10.1039/C5AY02014J

[163] Romero CP, Jeldres RI, Quezada GR, Concha F, Toledo PG. Zeta potential and viscosity of colloidal silica suspensions: Effect of seawater salts, pH, flocculant, and shear rate. Colloids Surf A Physicochem Eng Asp 2018;538:210–8. https://doi.org/10.1016/j.colsurfa.2017.10.080

[164] Li S, Leroy P, Heberling F, Devau N, Jougnot D, Chiaberge C. Influence of surface conductivity on the apparent zeta potential of calcite. J Colloid Interf Sci 2016;468:262–75. https://doi.org/10.1016/j.jcis.2016.01.075

[165] Kobayashi M, Juillerat F, Galletto P, Bowen P, Borkovec M. Aggregation and Charging of Colloidal Silica Particles: Effect of Particle Size. Langmuir 2005;21:5761–9. https://doi.org/10.1021/la046829z

[166] Alexander GB. The Polymerization of Monosilicic Acid. J Am Chem Soc 1954;76:2094–6. https://doi.org/10.1021/ja01637a017

[167] Chan SH. A review on solubility and polymerization silica. Geothermics 1989;18:49–56. https://doi.org/10.1016/0375-6505(89)90009-6

[168] Icopini GA, Brantley SL, Heaney PJ. Kinetics of silica oligomerization and nanocolloid formation as a function of pH and ionic strength at 25°C. Geochim Cosmochim Acta 2005;69:293–303. https://doi.org/10.1016/j.gca.2004.06.038

[169] Schubert H. Nanobubbles, hydrophobic effect, heterocoagulation and hydrodynamics in flotation. Int J Miner Process 2005;78:11–21. https://doi.org/10.1016/j.minpro.2005.07.002

[170] Flint LR, Howarth WJ. The collision efficiency of small particles with spherical air bubbles. Chem Eng Sci 1971;26:1155–68. https://doi.org/10.1016/0009-2509(71)87002-1

[171] Yoon RH, Luttrell GH. The Effect of Bubble Size on Fine Particle Flotation. Min Proc Ext Met Rev 1989;5:101–22. https://doi.org/10.1080/08827508908952646

[172] Hampton MA, Nguyen AV. Nanobubbles and the nanobubble bridging capillary force. Adv Colloid Interf Sci 2010;154:30–55. https://doi.org/10.1016/j.cis.2010.01.006

[173] Tao D. Role of Bubble Size in Flotation of Coarse and Fine Particles—A Review. Sep Sci Technol 2004;39:741–60. https://doi.org/10.1081/SS-120028444

[174] Brown K, Dunstall M. Silica scaling under controlled hydrodynamic conditions. Proceedings of World Geothermal Congress; 2000; Kyushu – Tohoku, Japan; 2000. 3039–44.

[175] Dunstall M, Zipfel H, Brown K. The Onset of Silica Scaling Around Circular Cylinders. Proceedings of World Geothermal Congress; 2000; Kyushu – Tohoku, Japan; 2000. 3045–50.

[176] van den Heuvel DB, Gunnlaugsson E, Benning LG. Surface roughness affects early stages of silica scale formation more strongly than chemical and structural properties of the substrate. Geothermics 2020;87:101835. https://doi.org/10.1016/j.geothermics.2020.101835